Facile construction & modeling of a highly active thiacalixphenyl[4]arene-protected nano-palladium catalyst for various C-C cross-coupling reactions

Krunal Modi,*[a] Chirag Patel[b] , Urvi Panchal[c], Alan Liska [a], Anita Kongor[c], Ludvik Jiri [a] and V.K.Jain[c]

[a.] *Department of Molecular Electrochemistry and Catalysis, J. Heyrovský Institute of Physical chemistry, Dolejškova 2155/3, 182 23 Prague 8, Czech Republic. Email: kmodi5033@gmail.com*
[b.] *Department of Botany, Bioinformatics and Climate Change Impacts Management, University School of Sciences, Gujarat University, Ahmedabad – 380009, Gujarat, India.*
[c.] *Department of Chemistry, University School of Sciences, Gujarat University, Ahmedabad – 380009, Gujarat, India.*

Supplementary information

S1 Mass of TPTEA
S2 ^{1}H NMR of TPTEA
S3 ^{13}C NMR of TPTEA
S4 ^{13}C-DEPT NMR of TPTEA
S5 Mass of TPTAH
S6 ^{1}H NMR of TPTAH
S7 ^{13}C NMR of TPTAH
S8 ^{13}C-DEPT NMR of TPTAH
S9 Mass of 1,1'-biphenyl(Table 1)
S10 ^{1}H NMR of 1,1'-biphenyl(Table 1)
S11 Mass of Entry 1(Table 2)
S12 ^{1}H NMR of Entry 1(Table 2)
S13 Mass of Entry 2(Table 2)
S14 ^{1}H NMR of Entry 2(Table 2)
S15 Mass of Entry 3(Table 2)
S16 ^{1}H NMR of Entry 3(Table 2)
S17 Mass of 1,2-diphenylethene(Table 3)
S18 ^{1}H NMR of 1,2-diphenylethene(Table 3)
S19 Mass of Entry 1(Table 4)
S20 ^{1}H NMR of Entry 1(Table 4)
S21 Mass of Entry 2(Table 4)
S22 ^{1}H NMR of Entry 2(Table 4)
S23 Mass of Entry 3(Table 4)
S24 ^{1}H NMR of Entry 3(Table 4)
S25 Mass of 1,1'-biphenyl(Table 5)
S26 ^{1}H NMR of 1,1'-biphenyl(Table 5)
S27 Mass of Entry 1(Table 6)
S28 ^{1}H NMR of Entry 1(Table 6)
S29 Mass of Entry 2(Table 6)
S30 ^{1}H NMR of Entry 2(Table 6)
S31 Mass of Entry 3(Table 6)
S32 ^{1}H NMR of Entry 3(Table 6)
S33 Optimization details
S34 Mapped Molecular Electrostatic potential from the electron density (total SCF density; isoval=0.0004) (a) Front view, (b) Bottom view of various atoms of TPA at B3LYP/6-311G (d,p) level
S35 Mapped Molecular Electrostatic potential from the electron density (total SCF density; isoval=0.0004) (a) Front view, (b) Bottom view of various atoms of TPTAE at B3LYP/6-311G (d,p) level
S36 Natural Bond Orbital (NBO) charges of various atoms of TPTAH at B3LYP/6-311G (d,p) level
S37 Natural Bond Orbital (NBO) charges of various atoms of (a) TPA, (b) TPTAE at B3LYP/6-311G (d,p) level
S38 Natural Bond Orbital (NBO) charges of various atoms of TPA at B3LYP/6-311G (d,p)
S39 Natural Bond Orbital (NBO) charges of various atoms of TPTAE at B3LYP/6-311G (d,p)
S40 Natural Bond Orbital (NBO) charges of various atoms of TPTAH at B3LYP/6-311G (d,p)
S41 TPTAH_PdNps interactions after DFT optimization at HF/6-31G (d,p) level of approximation
S42 Optimization details for TPTAH_PdNps

S43 Geometry optimization graph of Total energy of TPTAH_PdNps@ HF/Gen

S44 Geometry optimization graph of RMS Gradient Norm of TPTAH_PdNps@ HF/Gen

S45 Simulation interaction analysis through RMSD (Root mean square deviation of a ligand); rGyr (Radius of Gyration); intra Hydrogen bond; MolSA (Molecular Surface Area); SASA (Solvent Accessible Surface Area) and PSA (Polar Surface Area)

S46 TPTAH_PdNps donor-acceptor interactions and atom charges after DFT optimization at HF/6-31G (d,p) level of approximation

S47 UV-Vis Spectra of TPTAH, TPTAH-PdNPs, and PdAc.

Materials and Instrumentation

All alkyl halides, phenylboronic acid, trichloro(phenyl) stannane, styrene, and other reagents were purchased from Sigma-Aldrich Chemical Co., Ltd., India. Analytical grade chemicals were used for this work and without further purification. Thin layer chromatography was carried out on silica gel 60 F_{254} silica-aluminum plates, and the plates were visualized using ultraviolet light.

All the glassware was dried overnight in an oven before use. The mass analyses were performed using the ESI technique on a Q-TOF (micromass) spectrometer. NMR data were collected using a Bruker AV(III) 400 MHz with a BBFO probe. All samples were analyzed in $CDCl_3$ and $(CD_3)_2SO$. The reference values for residual solvent were taken as δ=7.27($CDCl_3$) and δ=2.5(DMSO) for ^{1}H-NMR and δ=77.1 ($CDCl_3$) and δ=40.0(DMSO) for ^{13}C-NMR. Multiplicities for coupled signals were designated using the abbreviations s=singlet, d=doublet, dd= doublet of doublets, ddd= doublet of doublet of doublets, and m= multiplets, and all frequencies are given in hertz. A VEEGO (Model No: VMP-DS) melting point apparatus (Mumbai, India) was used to measure the melting points (uncorrected) in a single capillary tube. Centrifugation of the colloidal solutions was performed using a Remi Model No. C-24BL laboratory centrifuge. The absorption spectra were recorded using a Jasco V-760 UV–vis recording spectrophotometer (Easton, US) with an EHCS-760 in the range of 200 – 800 nm. The TEM images were recorded on a JEOL model JEM 2100 using an acceleration voltage of 200 kV. The zeta potentials were obtained by a Malvern Zetasizer (Model ZEN3600) without dilution.

Insilico details

The quantum chemical calculation has been performed using Gaussian 09 program package (Revision A.01) [1]. The geometry optimization of thiacalixphenyl[4]arene **(TPA)**, thiacalixphenyl[4]arene tetra-ethylacetate **(TPTEA)**, thiacalixphenyl[4]arene tetra-acetohydrazide **(TPTAH)** was optimized at Hetree-fock and B3LYP level of theory.

Available crystallographic pattern of Palldium(Pd) was extracted from American Mineralogist Crystal Structure Database (AMCSD) and the unit cell was extended using the builder panel of Winmostar V8.018. The Desmond program was applied for the simulation of

nano-assembly with TIP3P water model solvated conditions [2]. These conditions were pertained to standard protocol including periodic orthorhombic box of dimension 10 Å×10 Å×10 Å with 58917 Å^3 Box volume or the OPLS_3 force field treatment [3, 4]. Energy minimization and equilibration of the solvated structure were achieved for the determination of native structure conformation. 50 nano seconds MD production time interval was retained with 300 K temperature and 50,000 iterations (for every 1 pico seconds). Nose–Hoover thermostat algorithm was applied with constant volume and shape ensemble (NVT) for the MD simulation process. Different interactions were monitored for the exploration of simulation using smooth particle mesh Ewald (PME) method (with a 10^{-9} tolerance limit) for long range interactions [5], while short range interactions were optimized at the 9 Å cut-off distance.

The geometry optimization of **TPTAH_PdNps** has been performed at Hatree-Fock level of approximation with [B3LYP/6-31 G(d,p)/SDD] basis sets. The C, H, N, O and S atoms were described by the 6-31 G(d,p), while SDD [6, 7] relativistic pseudopotential was used for the Palladium cluster. Vibration frequency calculations were performed to ensure that the optimized geometries represent local minima associated with positive eigen values only. The electrostatic potential is mapped onto a particular value of the total electron density (isovalue=0.004) using the Gauss view. Natural bond orbital (NBO) calculations were also performed at the same level of theory using Gaussian NBO Version 3.1 program to estimate the NBO charges due to second order interactions.

The single point energy calculations were carried out to calculate the strength of the complex in the term of binding energy. The binding energy of the TPTAH_PdNPs was calculated by energies as mentioned as in following equation.

$$\mathbf{BE} = \boldsymbol{E}_{\mathbf{(TPTAH\_PdNPs)}} - [\boldsymbol{E}_{\mathbf{(TPTAH)}} + \boldsymbol{E}_{\mathbf{(Pd\_Cluster)}}]$$

Where, $E_{(TPTAH\_PdNPs)}$ is the energy of the TPTAH_PdNPs and $E_{(TPTAH)}$ and $E_{(Pd\_Cluster)}$ are the energies of the TPTAH and Pd_Cluster, respectively. The donor-acceptor interaction and atom charge distribution visualize through discovery studio visualizer[8].

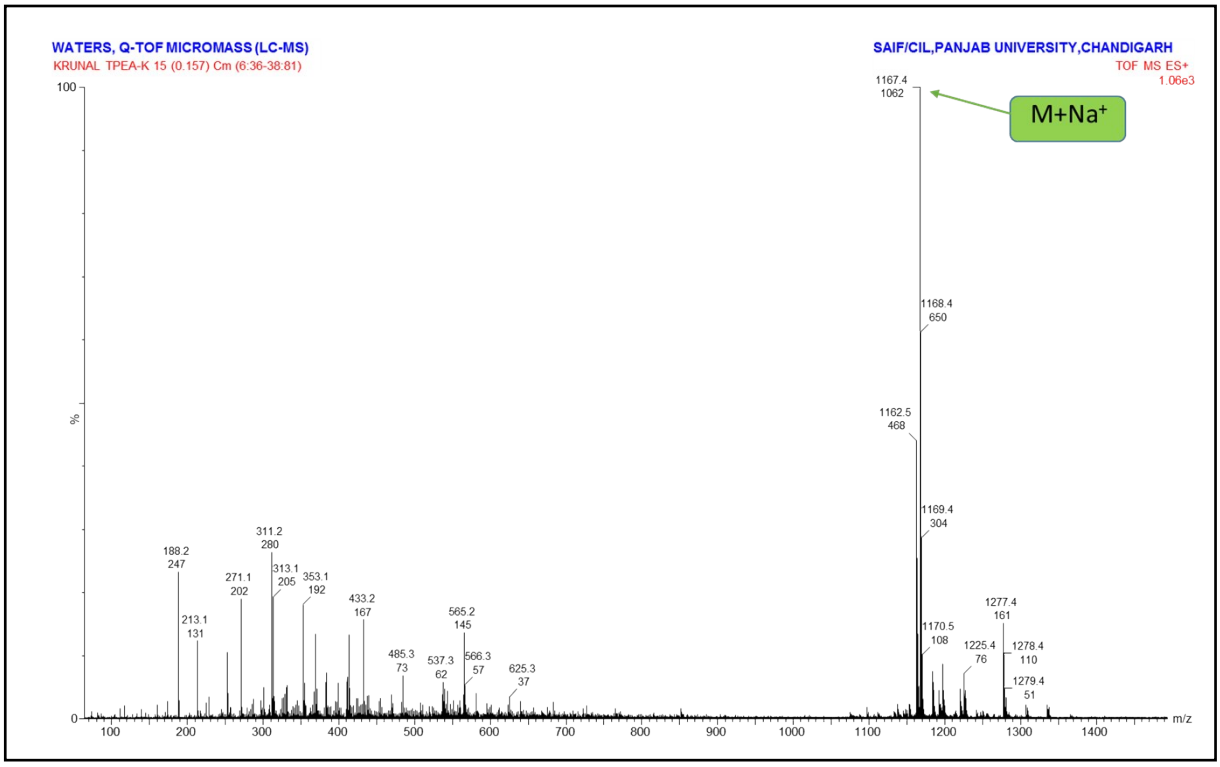

S1 Mass of TPTEA

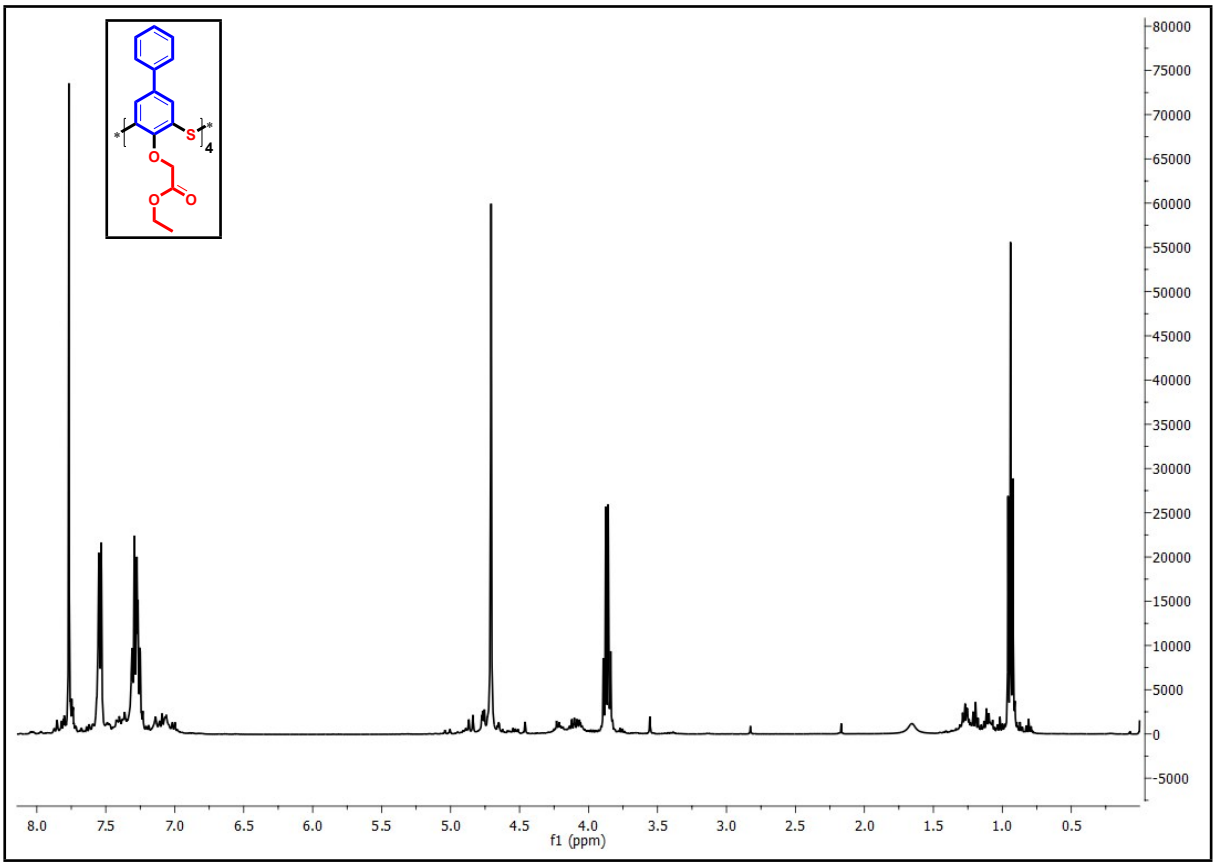

S2 ^{1}H NMR of TPTEA

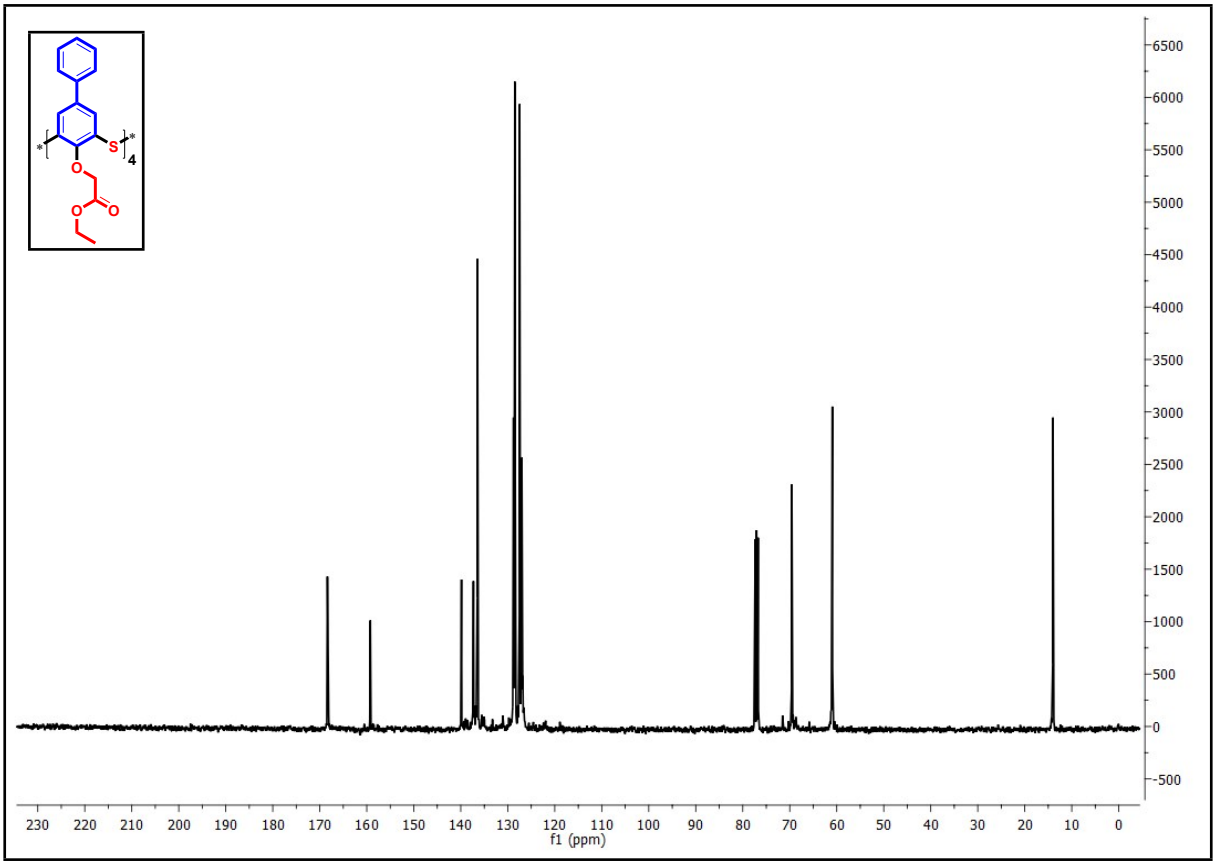

S3 ^{13}C NMR of TPTEA

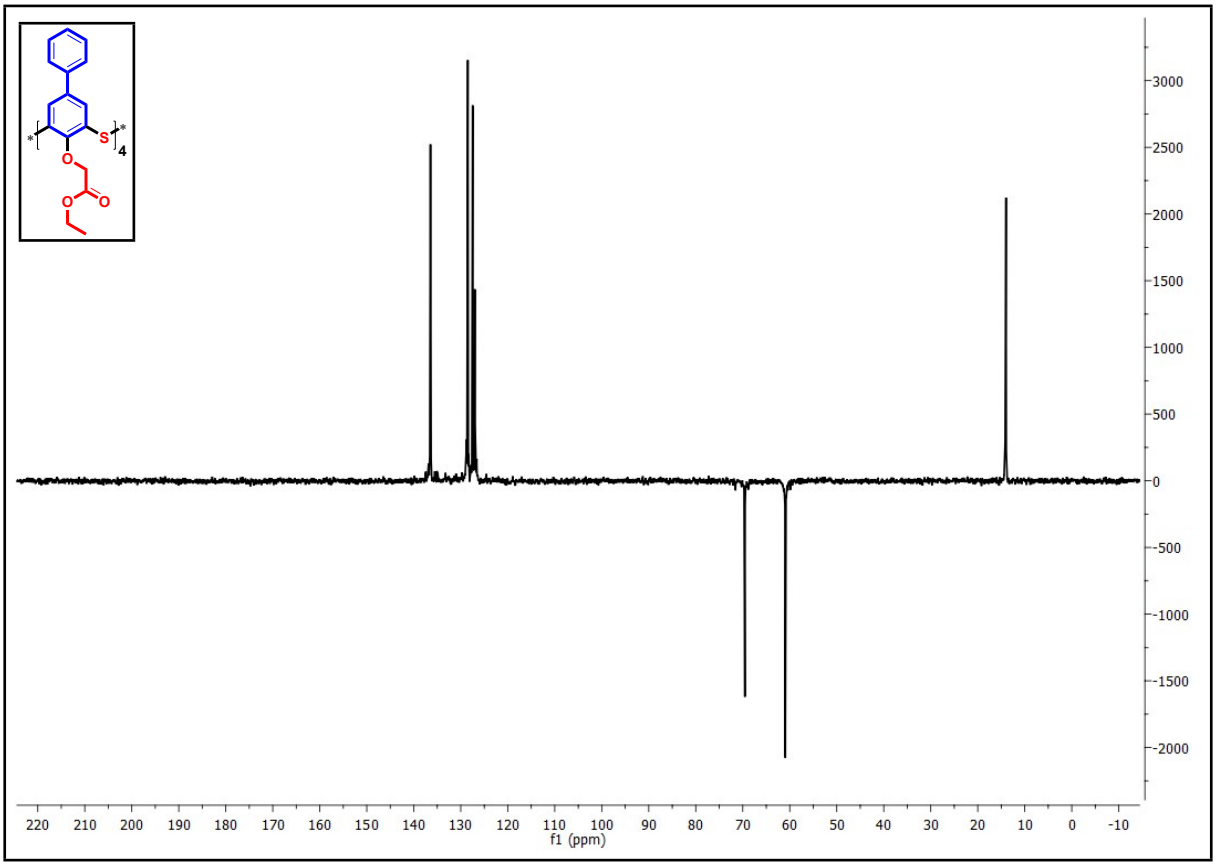

S4 ^{13}C-DEPT NMR of TPTEA

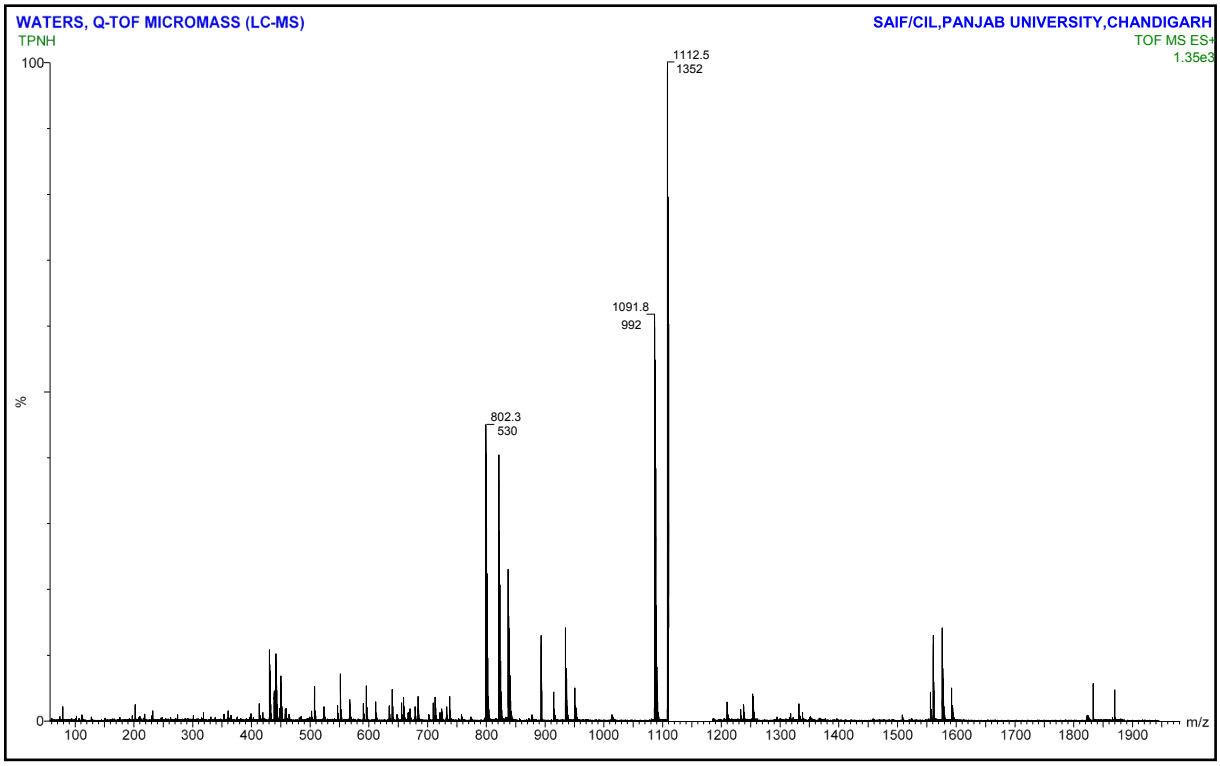

S5 Mass of TPTAH

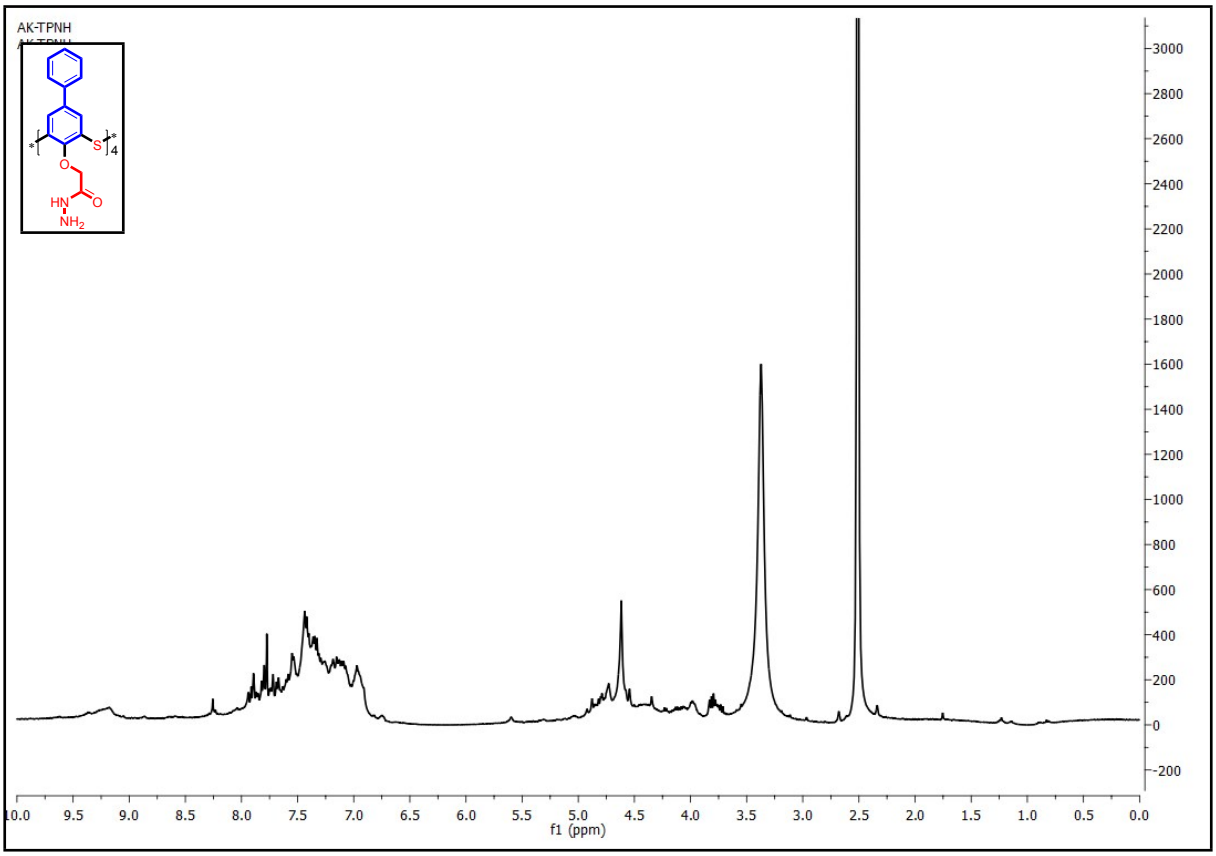

S6 ^{1}H NMR of TPTAH

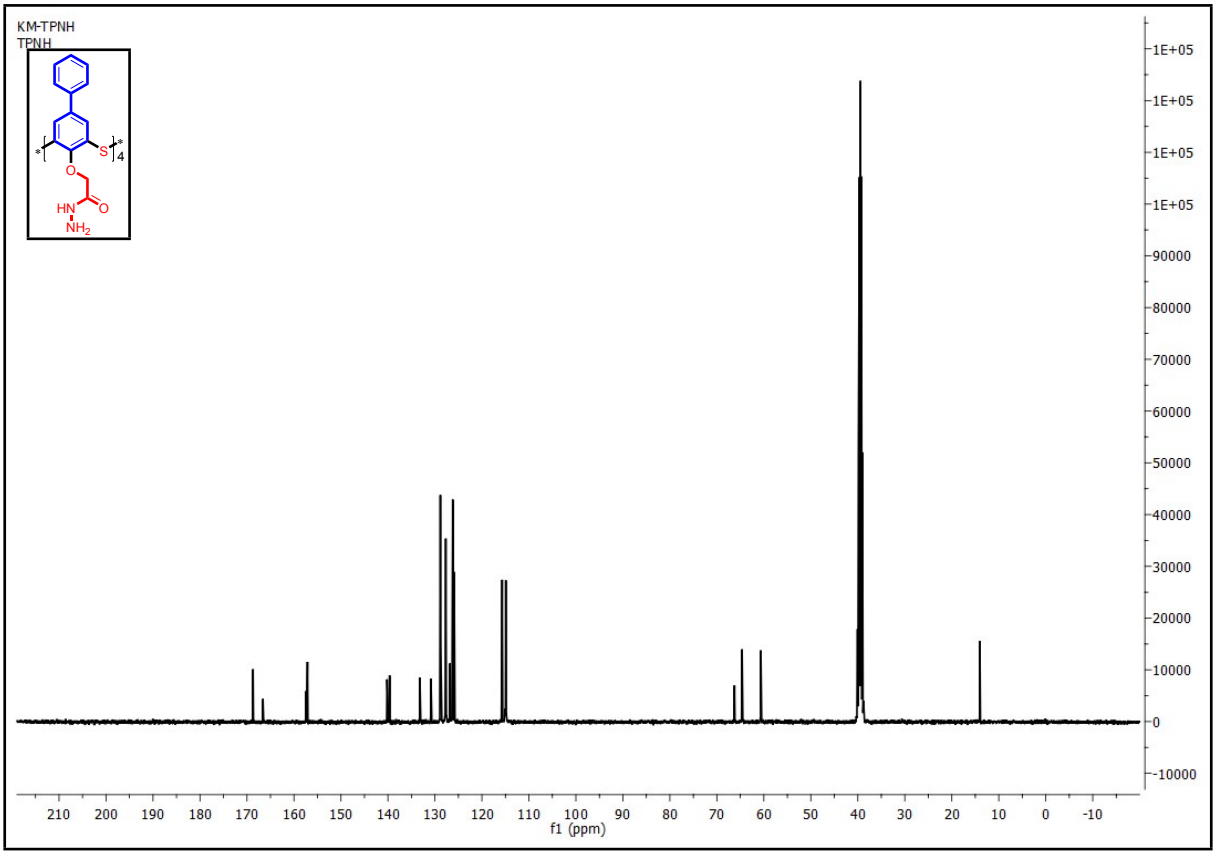

S7 ^{13}C NMR of TPTAH

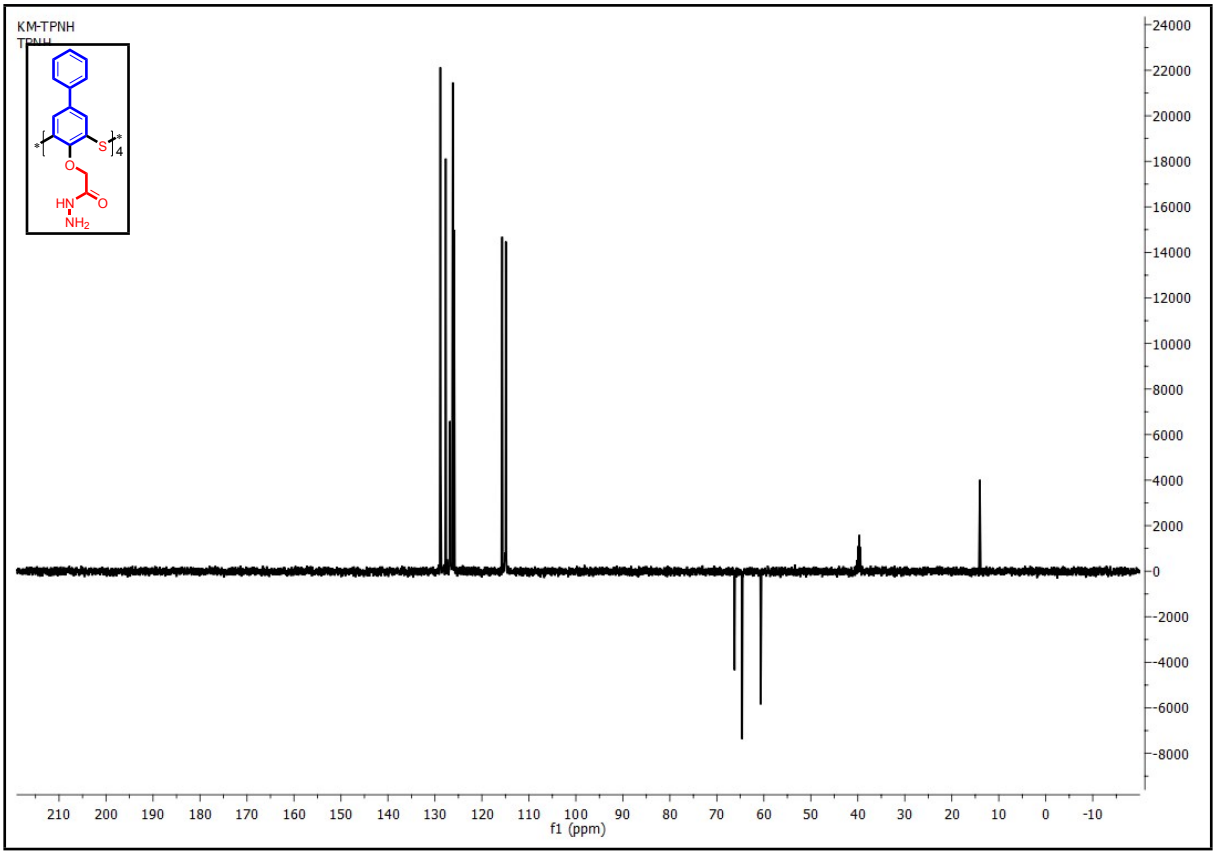

S8 ^{13}C-DEPT NMR of TPTAH

Characterization: Suzuki Cross-Coupling reaction				
Table	Entry	Figure	Mass	1H-NMR(400MHz, CDCl3) (δ ppm)
1	BP	16 & S17	172.18 $(M+H2O)^+$	7.28 (tt, 2H,Ar-H);7.37 (t, 4H,Ar-H);7.37 (dd, 4H,Ar-H)
2	1	S18 & S19	191.18 $(M+Na)^+$	2.53 (s, 3H,-CH3);7.36-7.39 (d, 2H,Ar-H);7.46 (t, 1H,Ar-H);7.56 (t, 2H,Ar-H);7.63-7.68 (d, 2H,Ar-H);7.71-7.73 (d, 2H,Ar-H)
	2	S20 & S21	186.5 $(M+2)^+$	3.77 (s, 3H,-CH3);6.89-6.92 (d, 2H,Ar-H);7.23 (t, 1H,Ar-H);7.34 (d, 2H,Ar-H);7.47 (d, 4H,Ar-H)
	3	S22 & S23	202.6 $(M+Na)^+$	7.34 (t, 1H,Ar-H);7.40 (tt, 2H,Ar-H);7.49-7.51 (dt, 2H,Ar-H);7.58-7.65 (m, 4H,Ar-H)

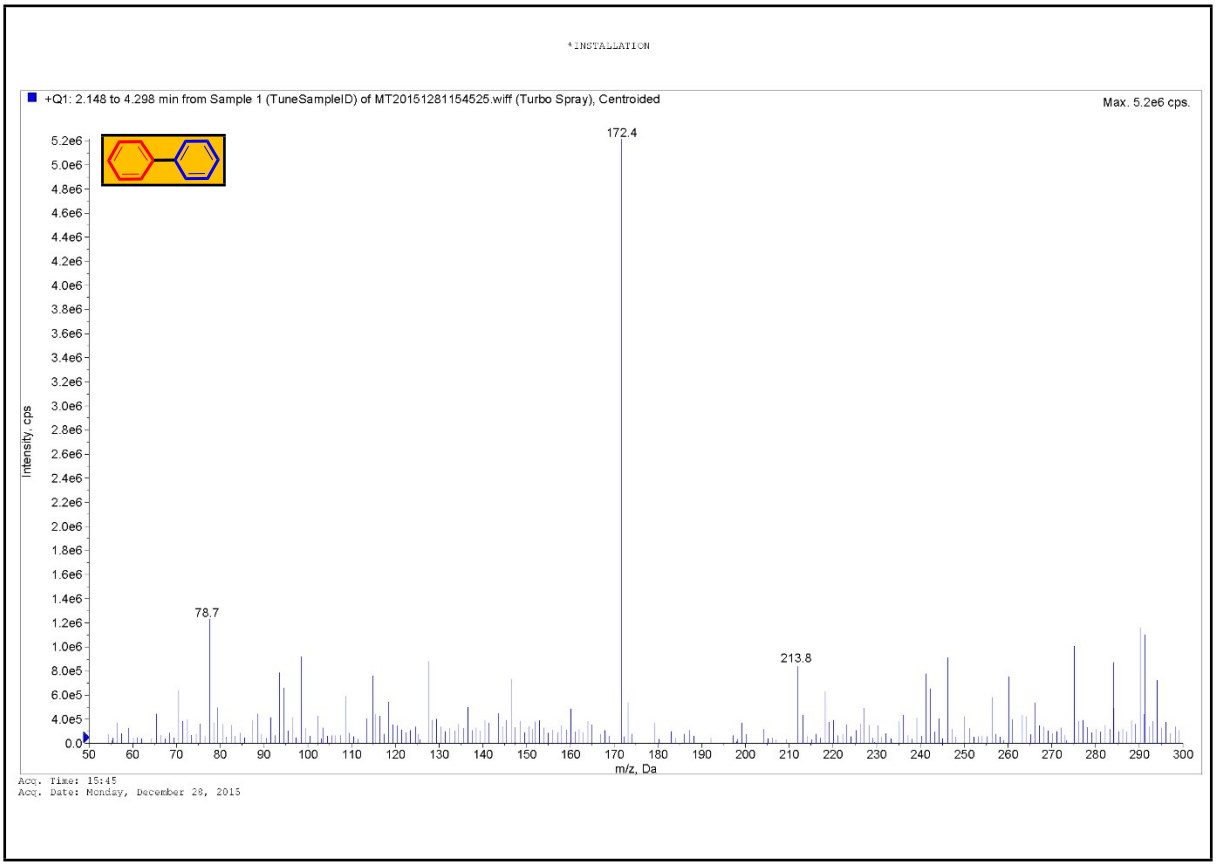

S9 Mass of 1,1'-biphenyl(Table 1)

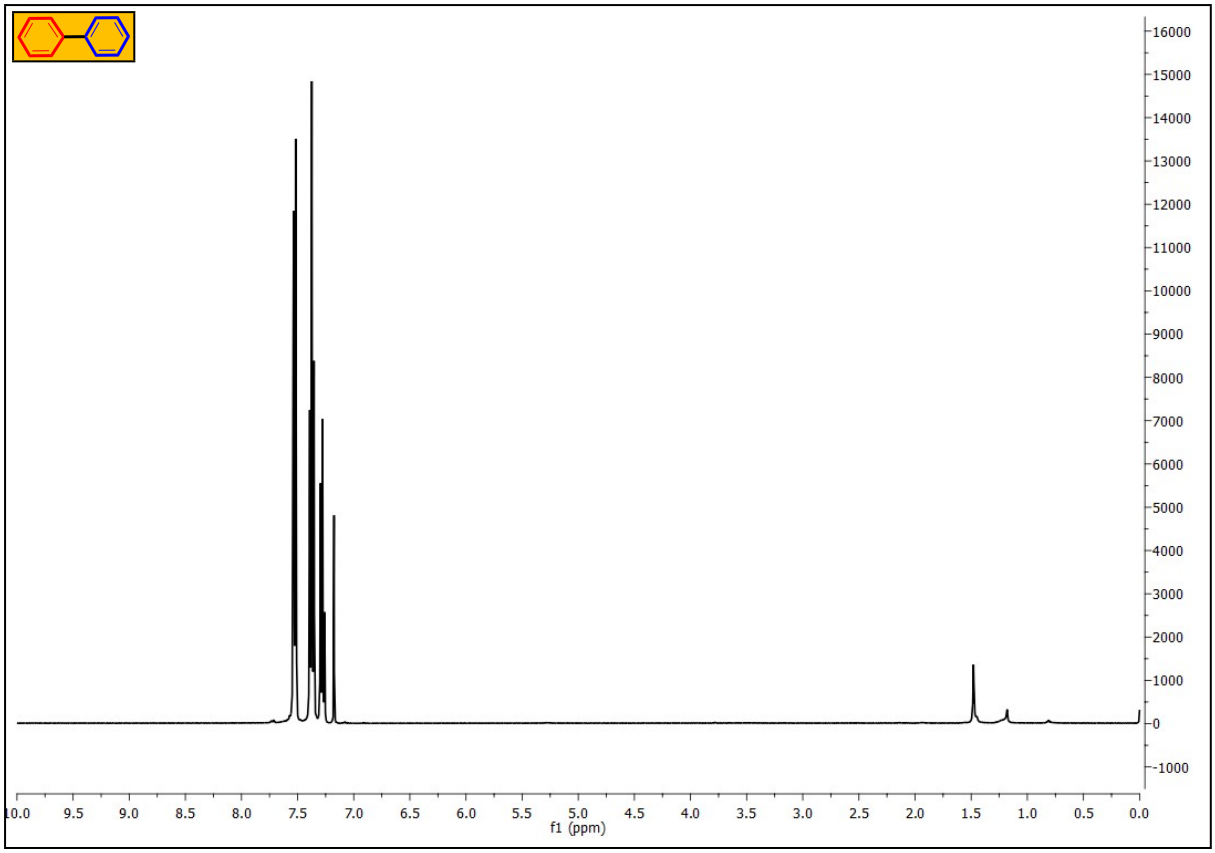

S10 ^{1}H NMR of 1,1'-biphenyl(Table 1)

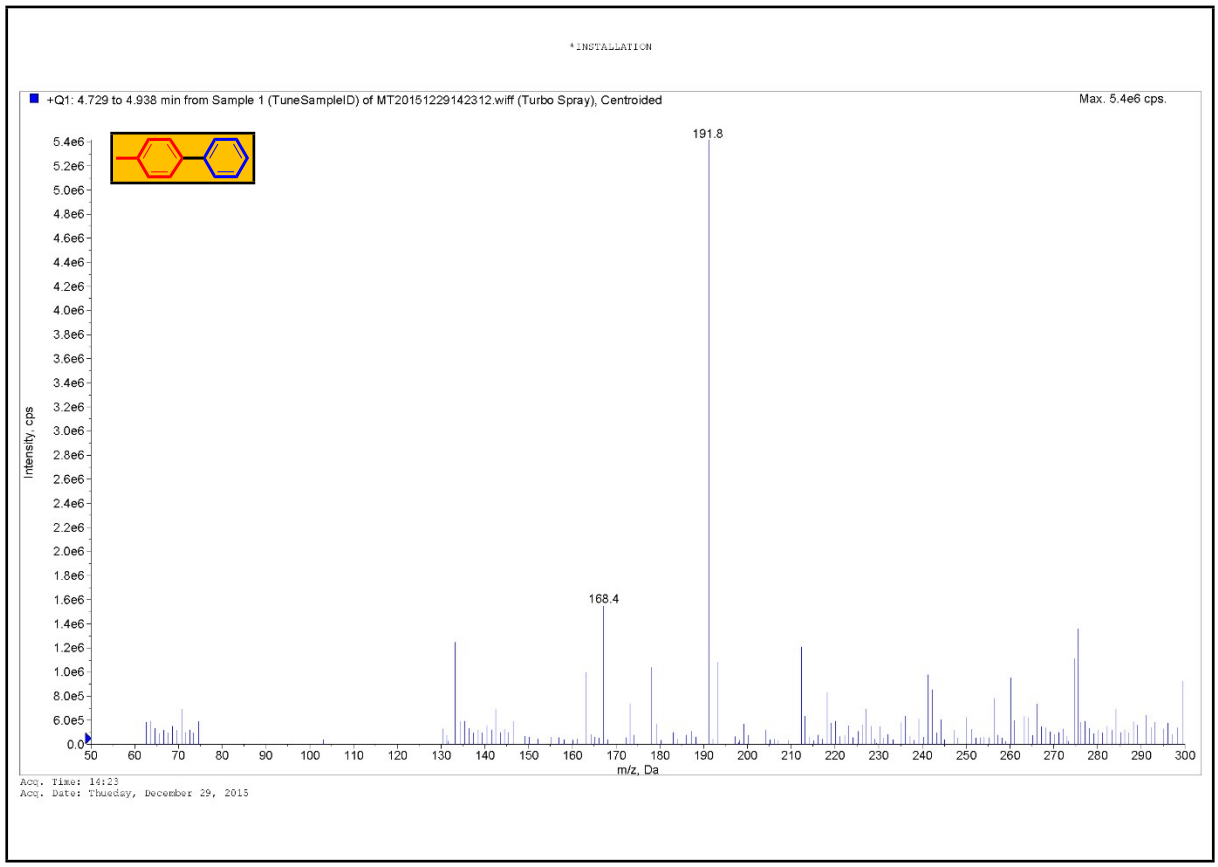

S11 Mass of Entry 1(Table 2)

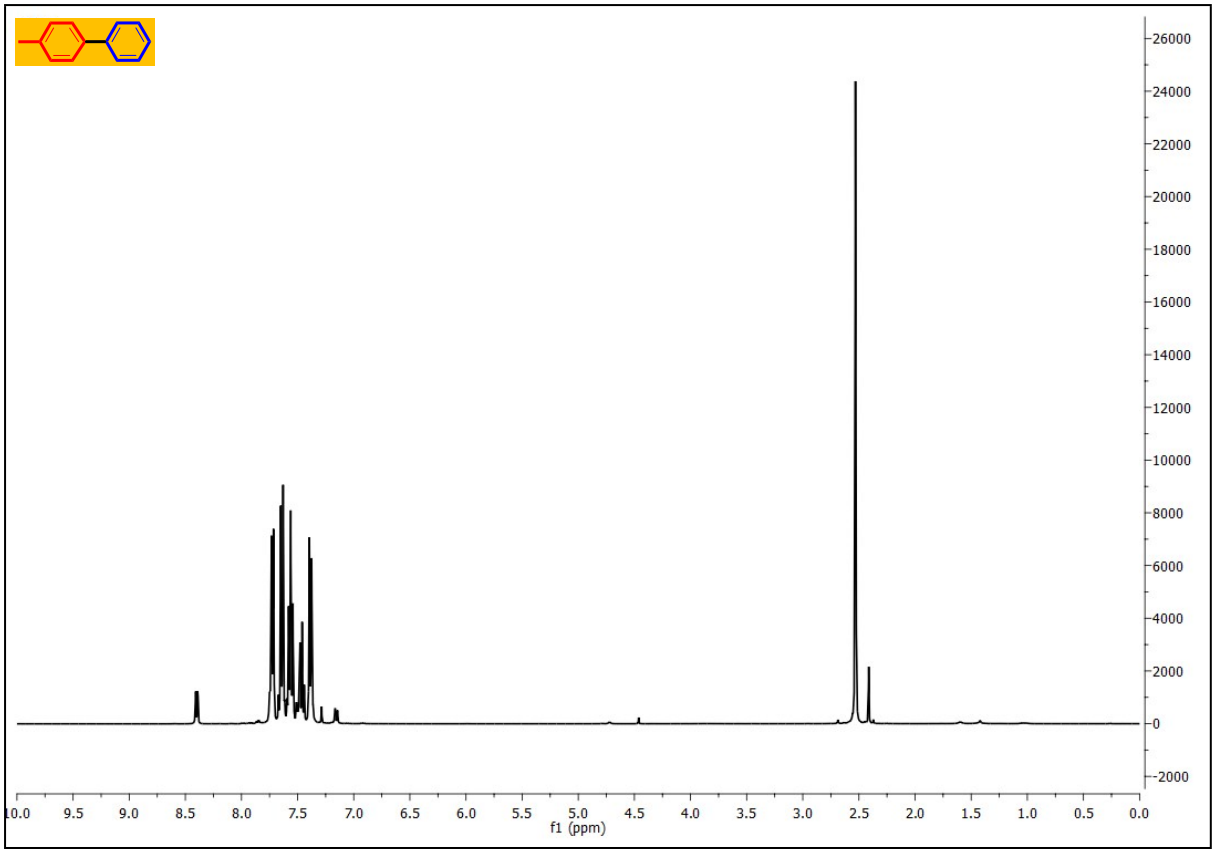

S12 ^{1}H NMR of Entry 1(Table 2)

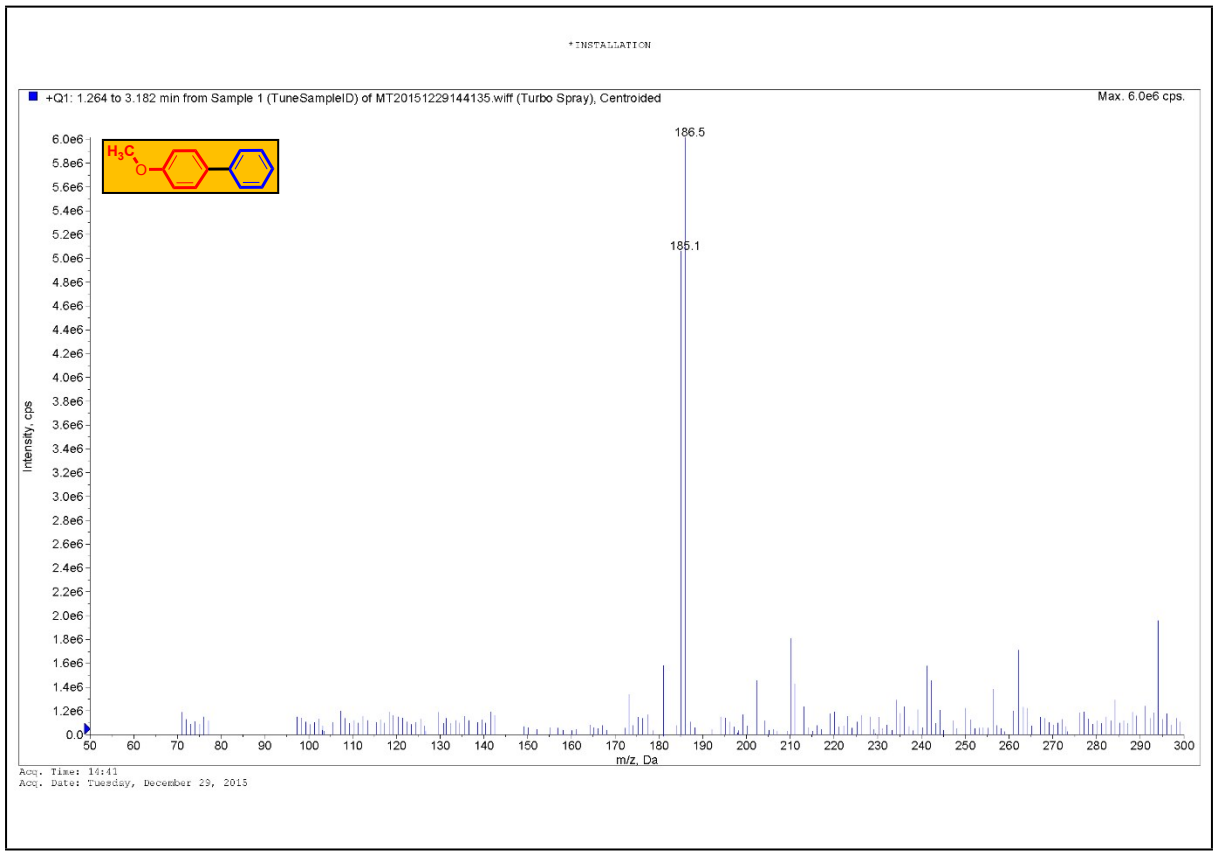

S13 Mass of Entry 2(Table 2)

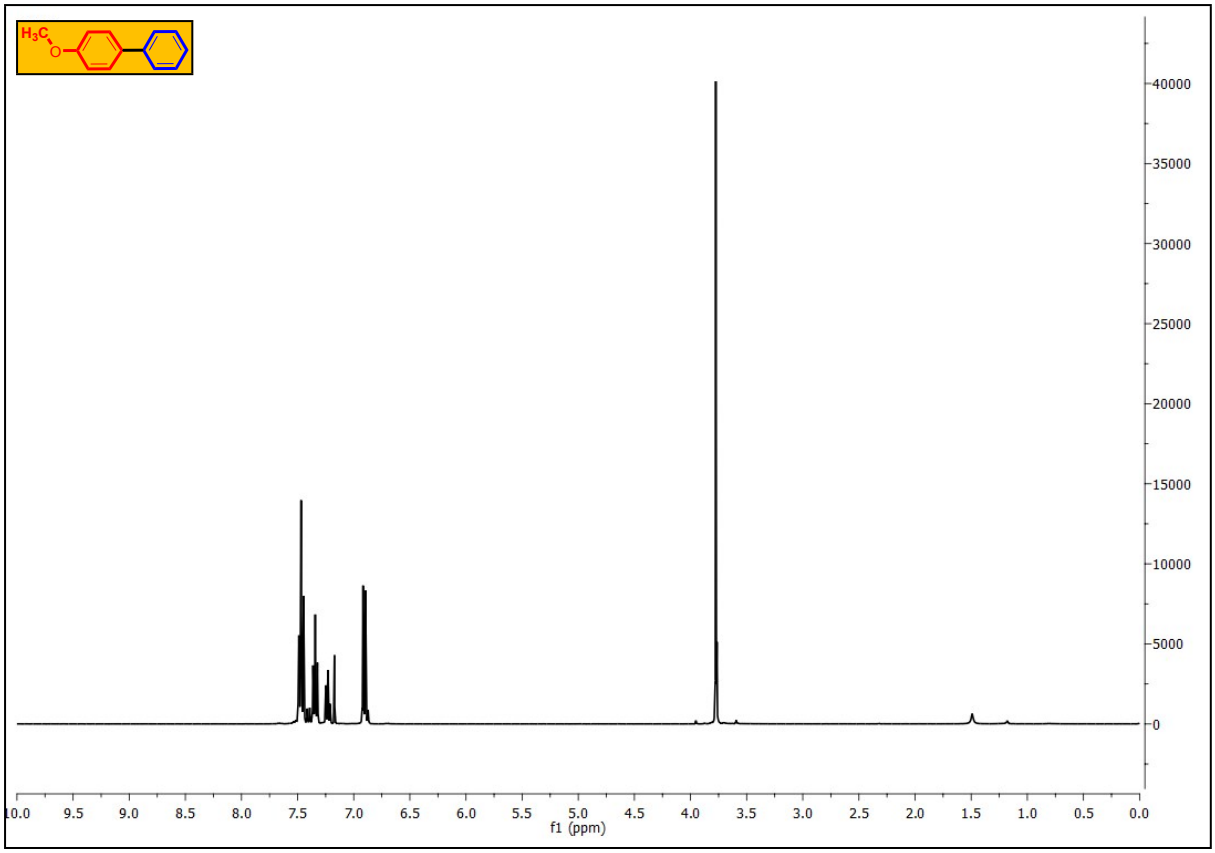

S14 ^{1}H NMR of Entry 2(Table 2)

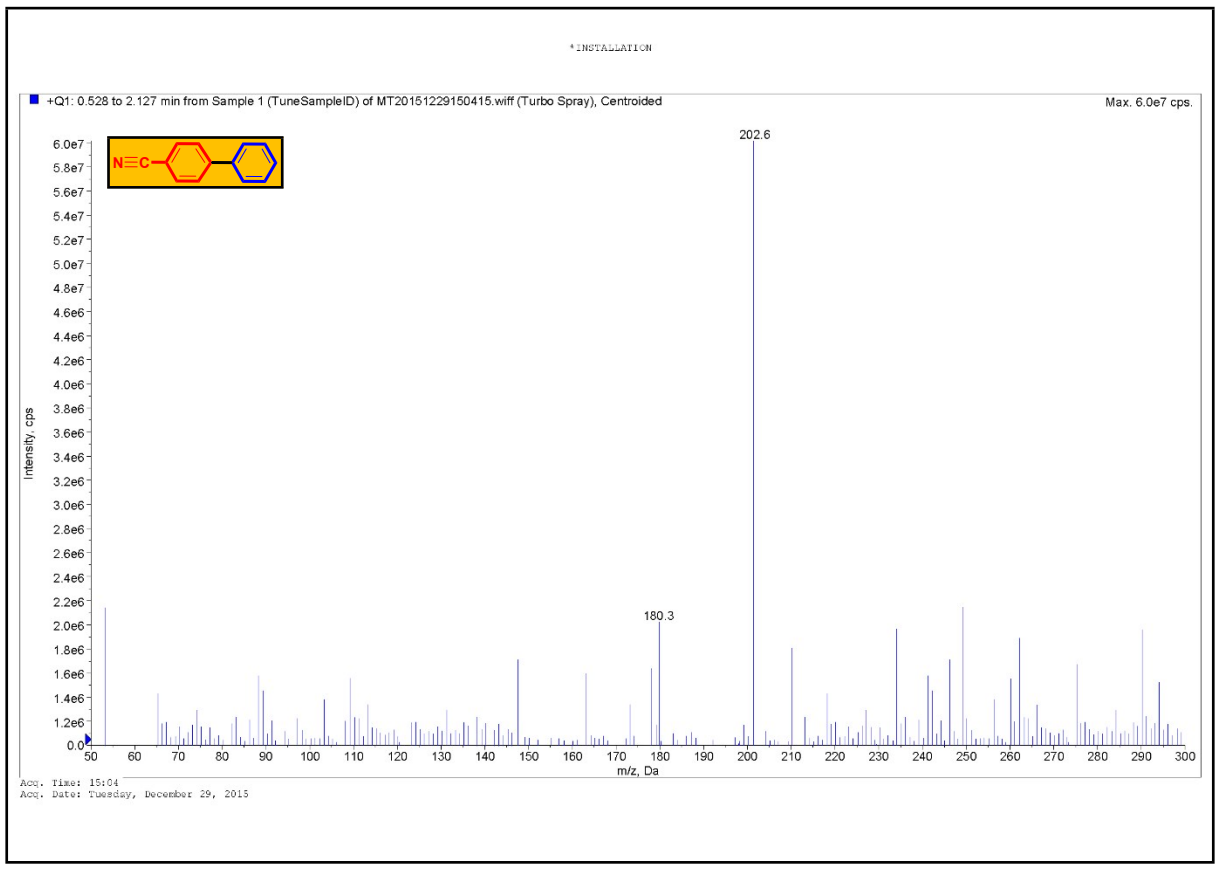

S15 Mass of Entry 3(Table 2)

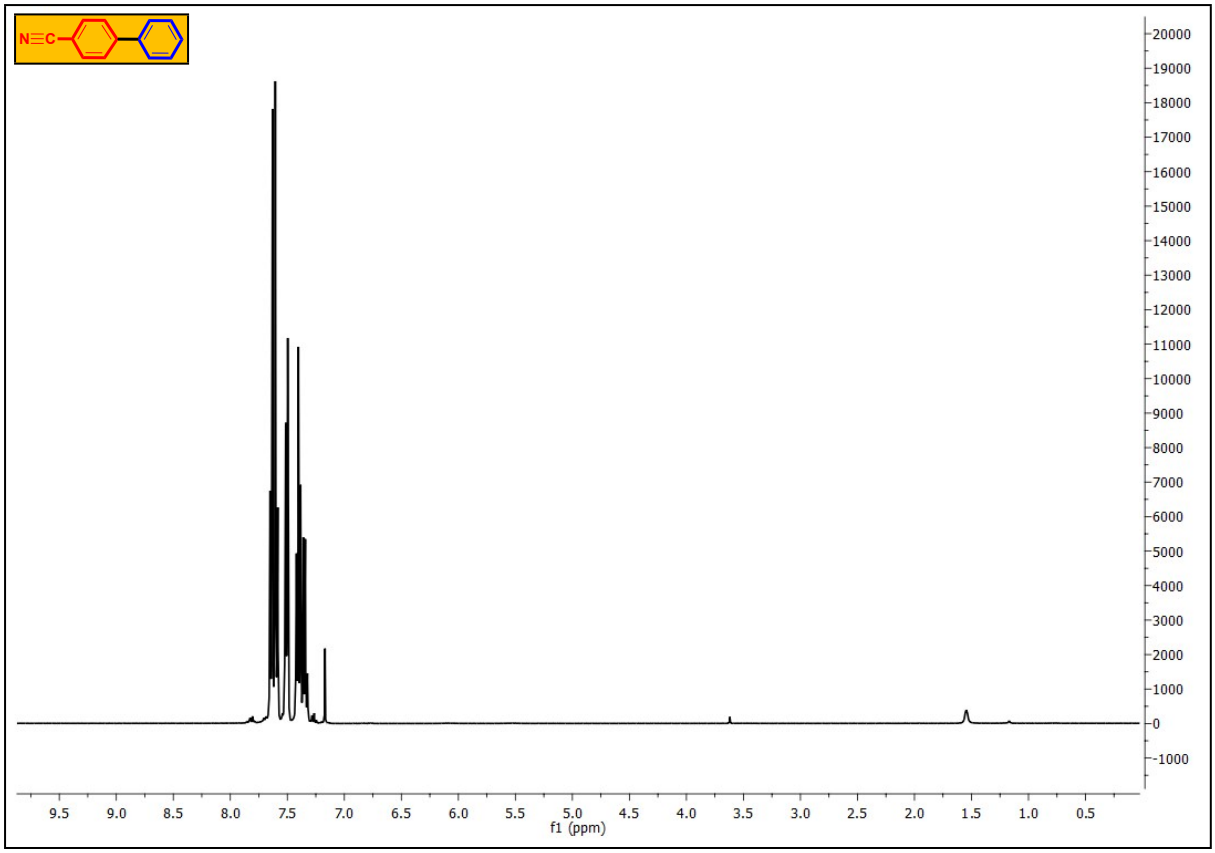

S16 ^{1}H NMR of Entry 3(Table 2)

Characterization: Heck Cross-Coupling reaction				
Table	Entry	Figure	Mass	1H-NMR(400MHz, CDCl3) (δ ppm)
3	DPE	S24 & S25	203.2(M+Na)+	7.21 (s, 2H,-CH=CH-);7.36 (d, 2H,Ar-H);7.46 (t, 4H,Ar-H);7.46 (t, 4H,Ar-H)
4	1	S26 & S27	219.2(M+Na)+	2.29 (s, 3H,-CH3);7.01 (s, 2H,-CH=CH-);7.11 (d, 2H,Ar-H);7.18 (d, 1H,Ar-H);7.28 (t, 2H,Ar-H);7.30-7.40 (d, 4H,Ar-H)
	2	S28 & S29	196.5(M+2)+	2.29 (s, 3H,-CH3);7.05 (s, 2H,-CH=CH-);7.11-7.18 (d, 3H,Ar-H); 7.20 (t, 2H,Ar-H);7.34-7.43 (d, 4H,Ar-H)
	3	S30 & S31	231.4(M+Na)+	7.16 (s, 2H,-CH=CH-);7.31 (t, 3H,Ar-H); 7.45 (d, 2H,Ar-H);7.56-7.79 (d, 4H,Ar-H); 9.90 (s, 1H,-CHO)

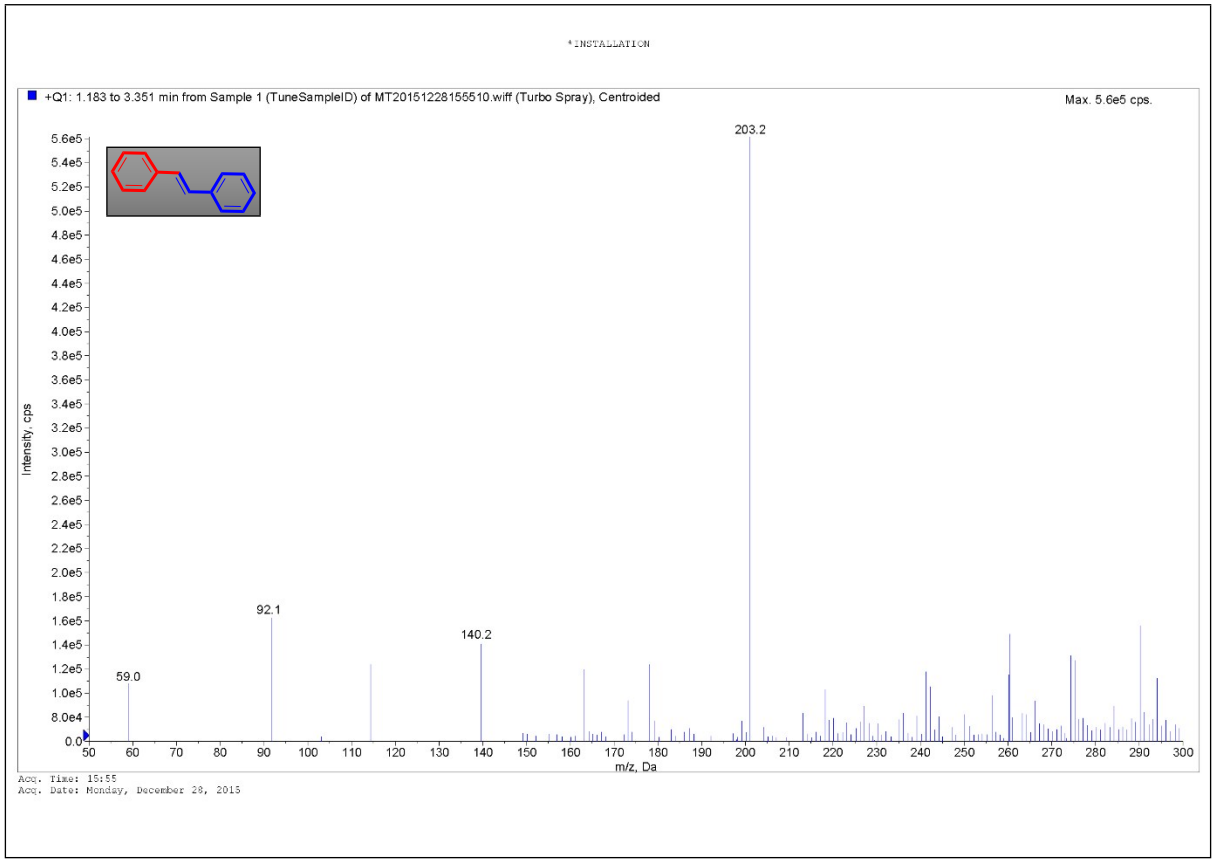

S17 Mass of 1,2-diphenylethene(Table 3)

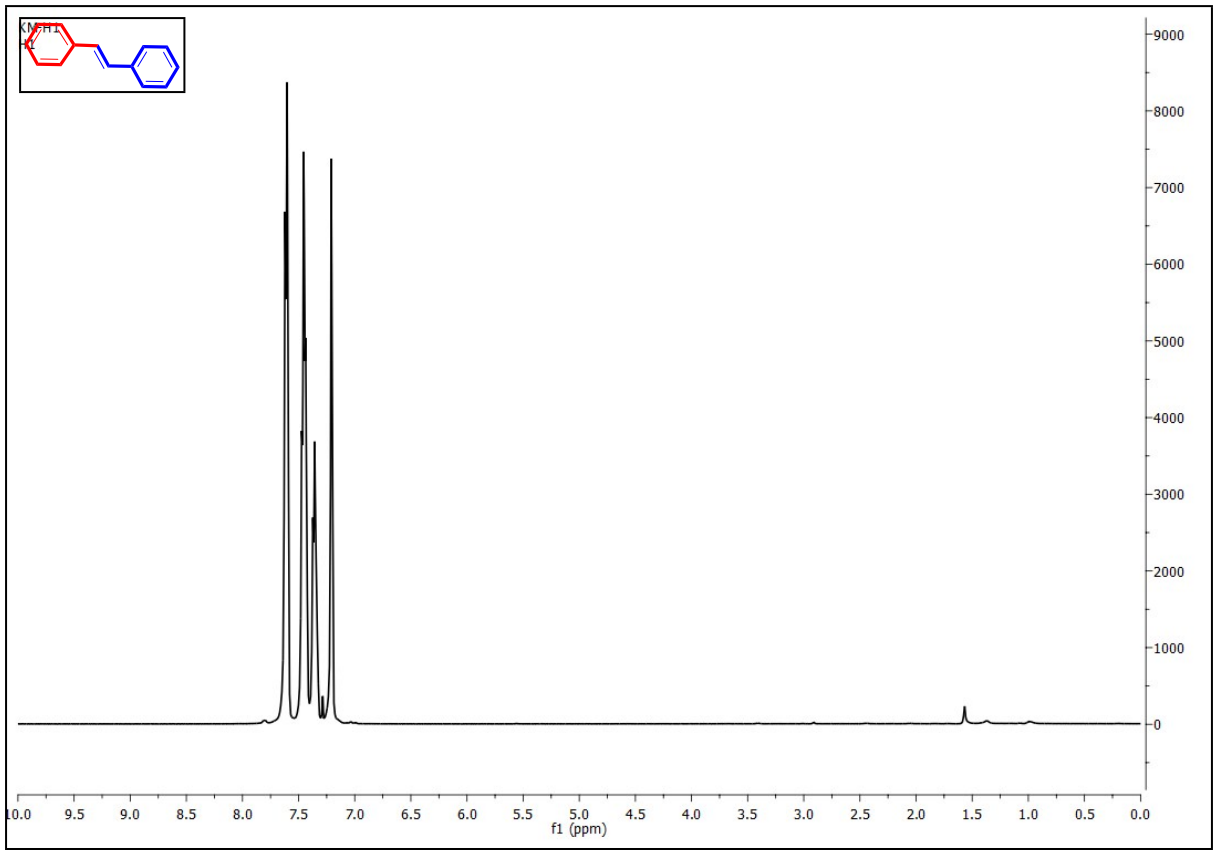

S18 ^{1}H NMR of 1,2-diphenylethene(Table 3)

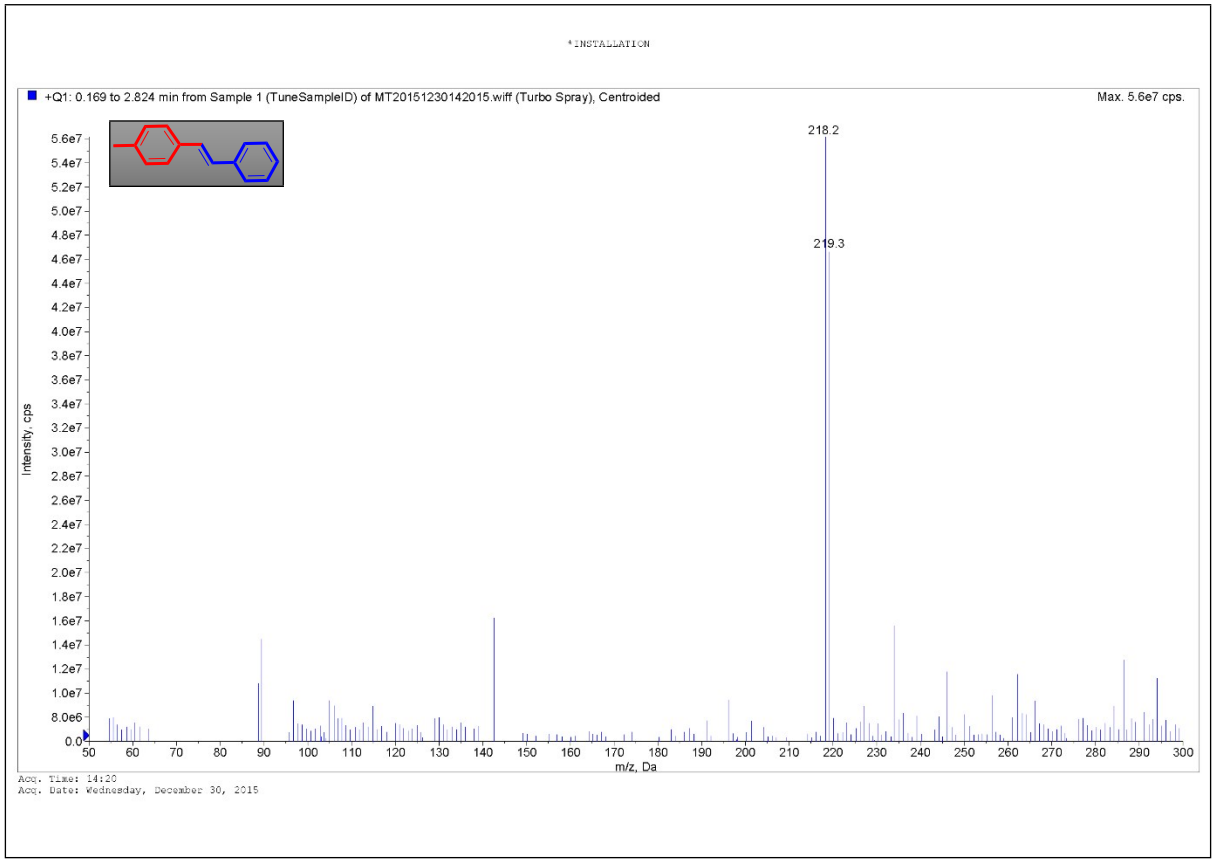

S19 Mass of Entry 1(Table 4)

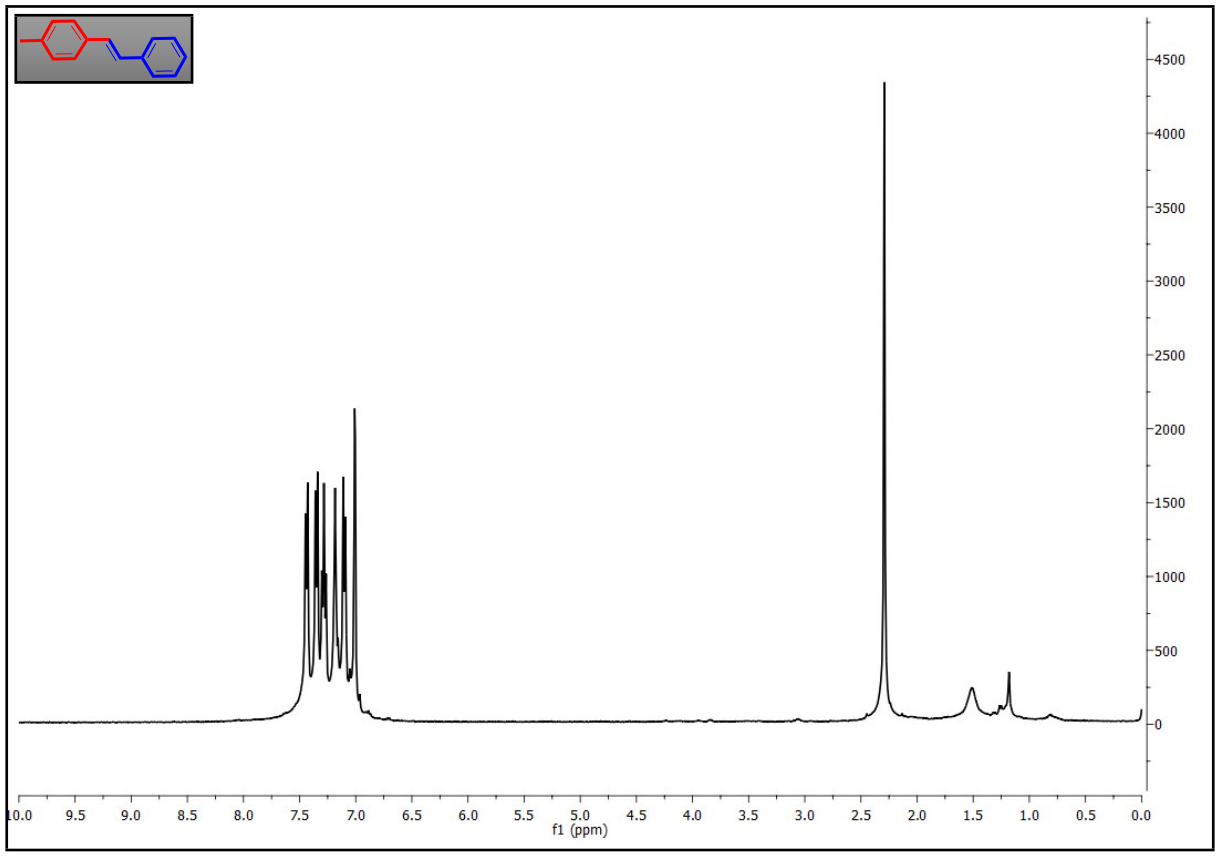

S20 ^{1}H NMR of Entry 1(Table 4)

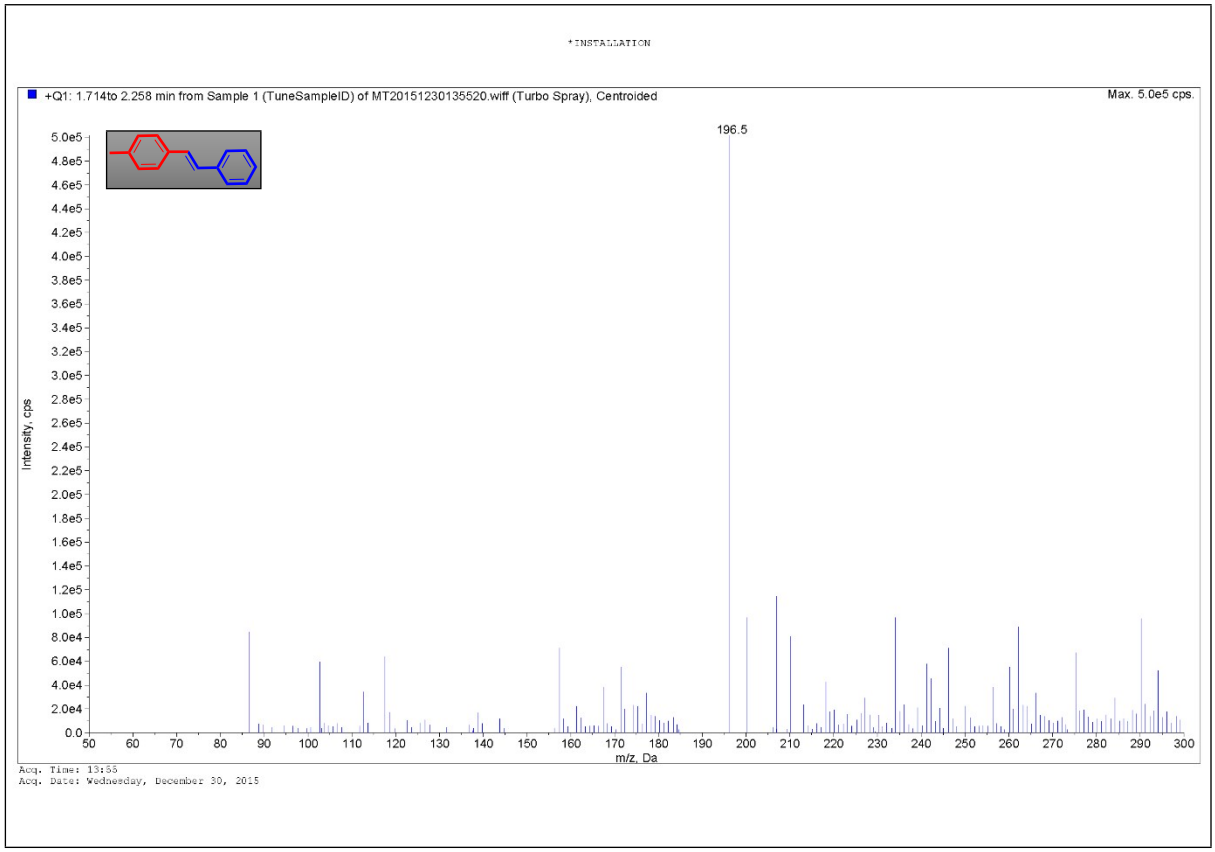

S21 Mass of Entry 2(Table 4)

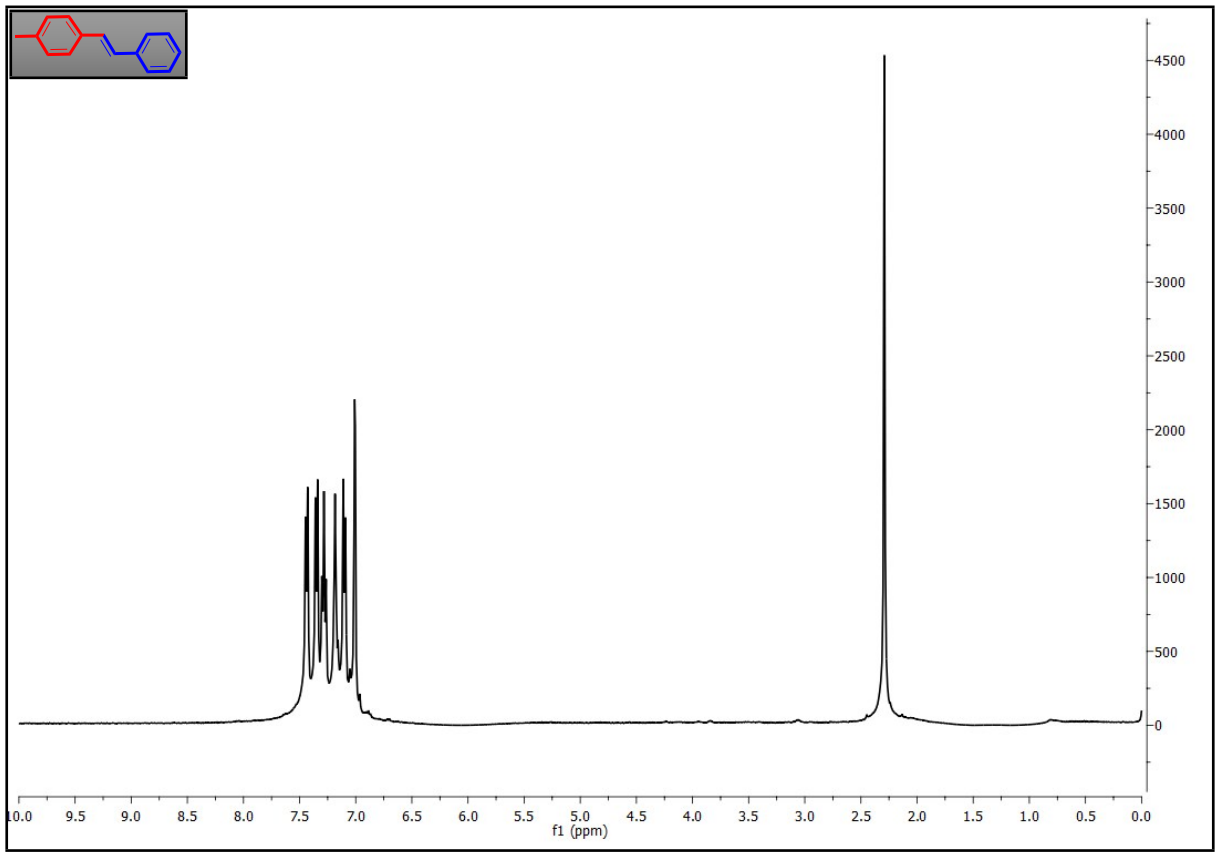

S22 ^{1}H NMR of Entry 2(Table 4)

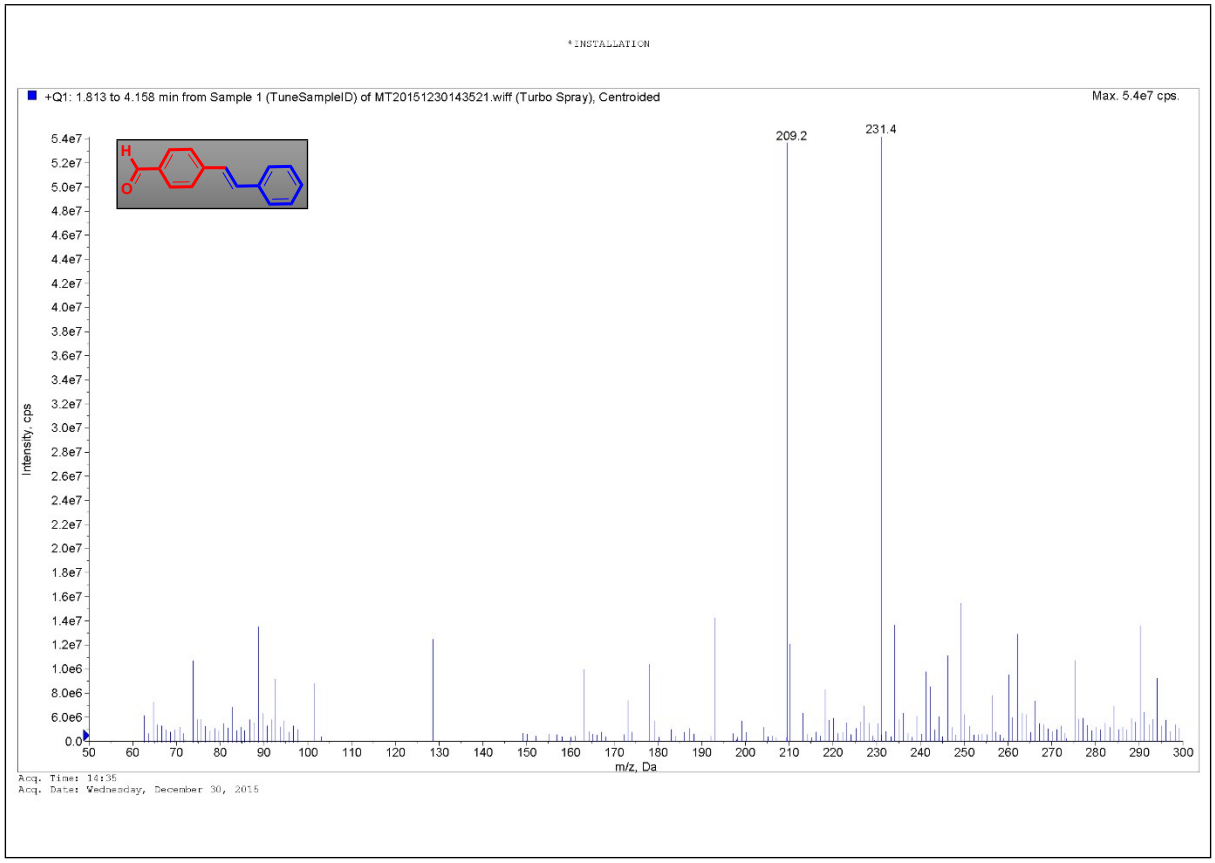

S23 Mass of Entry 3(Table 4)

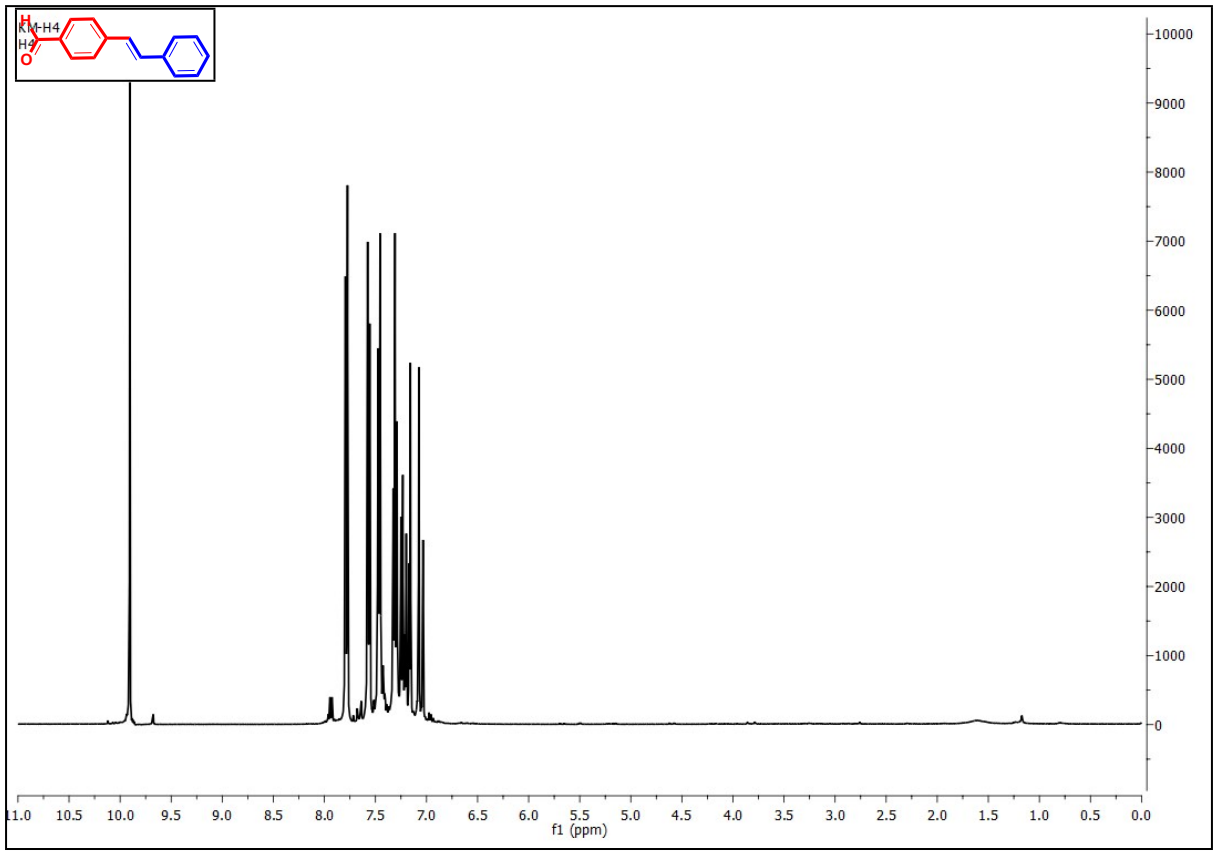

S24 ^{1}H NMR of Entry 3(Table 4)

Characterization: Stille Cross-Coupling reaction				
Table	Entry	Figure	Mass	1H-NMR(400MHz, CDCl3) (δ ppm)
5	BP	S32 & S33	177.8(M+Na)+	7.27 (t, 2H,Ar-H);7.36 (t, 4H,Ar-H);7.51 (d, 4H,Ar-H)
6	1	S34 & S35	170.4 (M+2)+	2.53 (s, 3H,-CH3);7.36 (d, 2H,Ar-H);7.43 (t, 1H,Ar-H);7.53 (t, 2H,Ar-H);7.60 (d, 2H,Ar-H);7.70 (d, 2H,Ar-H)
	2	S36 & S37	207.5(M+Na)+	3.76 (s, 3H,-O-CH3);6.89 (d, 2H,Ar-H);7.22 (t, 1H,Ar-H);7.34 (t, 2H,Ar-H);7.46 (t, 4H,Ar-H)
	3	S38 & S39	205.2(M+Na)+	7.51 (t, 3H,Ar-H);7.65 (d, 4H,Ar-H);7.88 (t, 1H,Ar-H);8.15 (t, 1H,Ar-H);10.10 (s, 1H,-CHO)

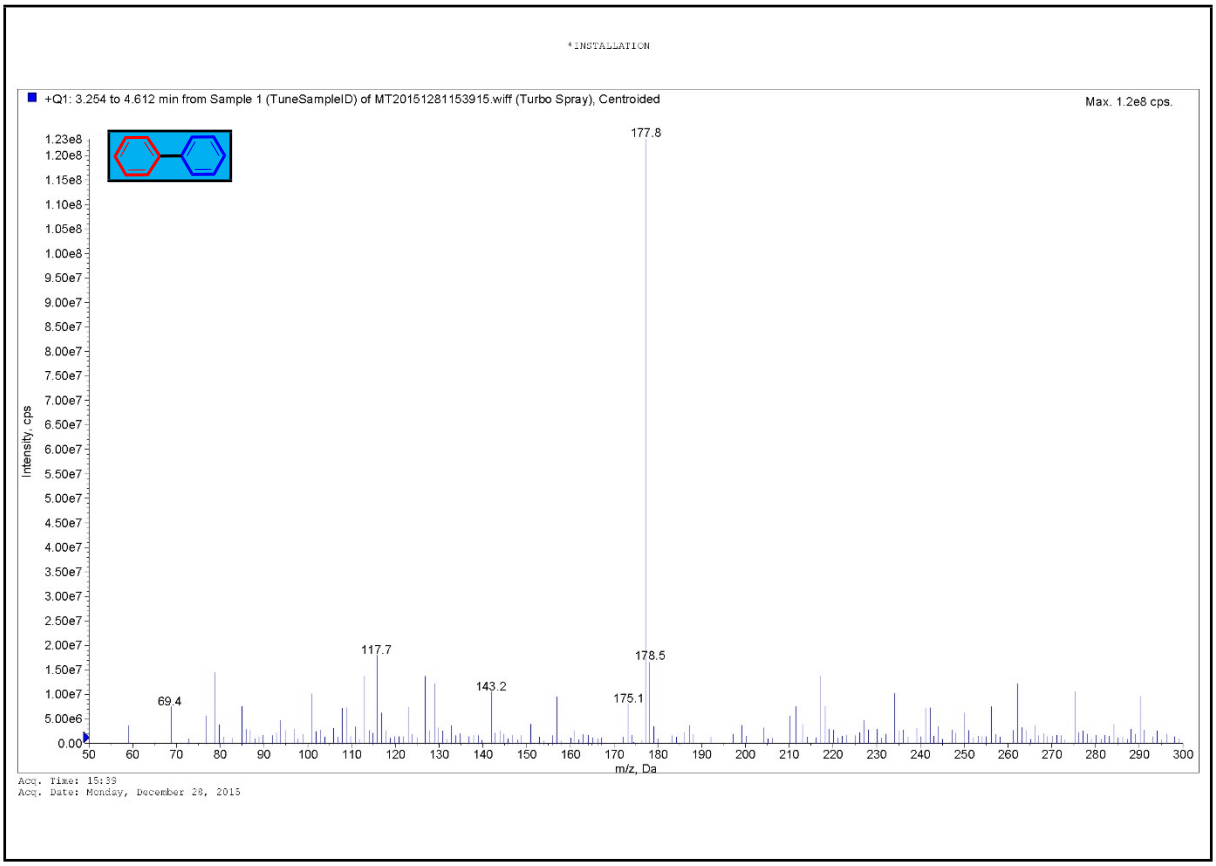

S25 Mass of 1,1'-biphenyl(Table 5)

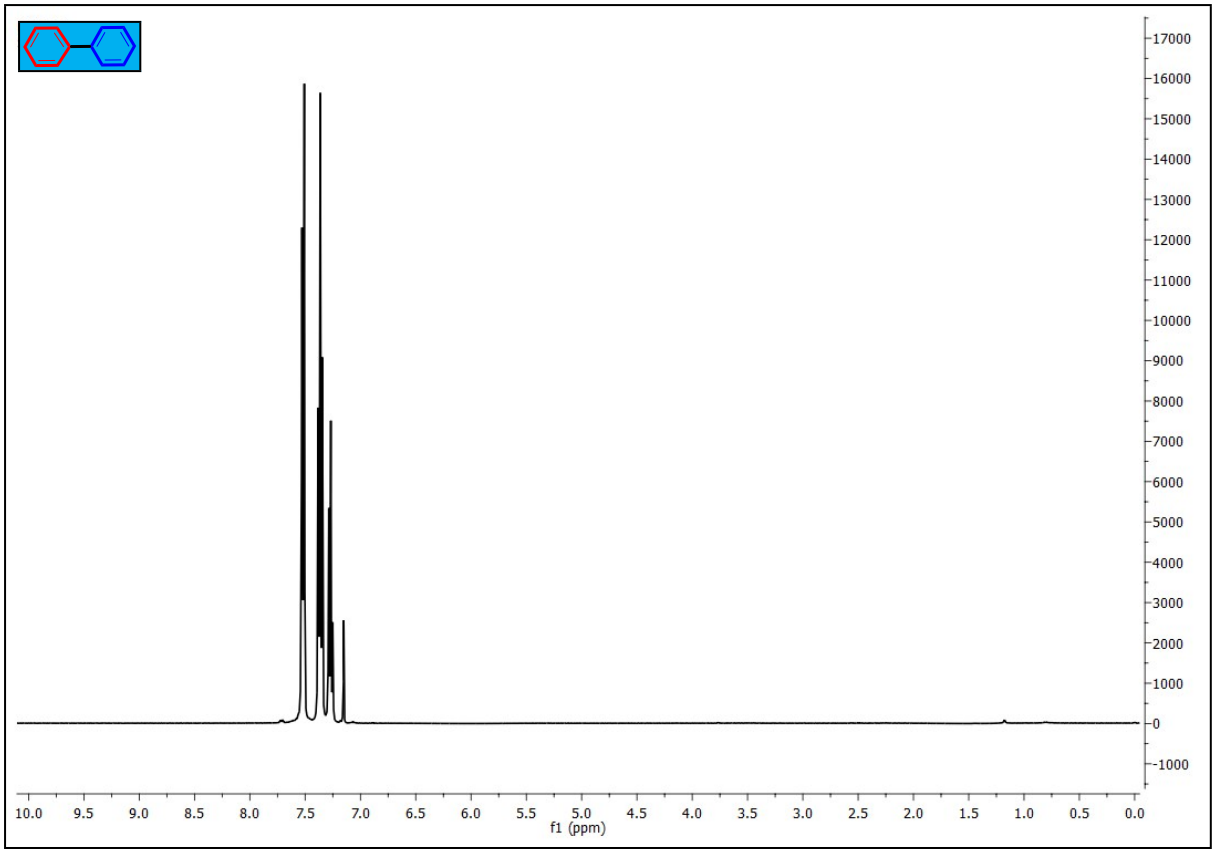

S26 ^{1}H NMR of 1,1’-biphenyl(Table 5)

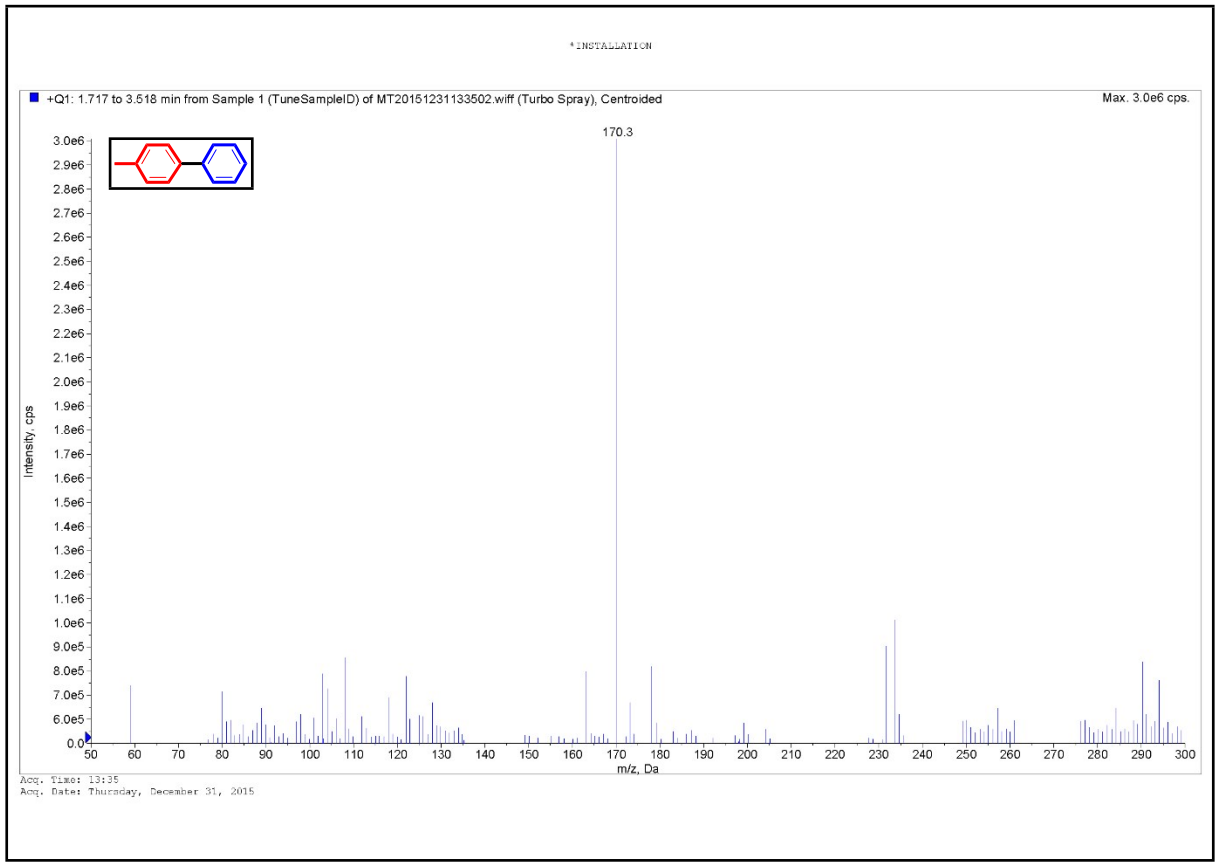

S27 Mass of Entry 1(Table 6)

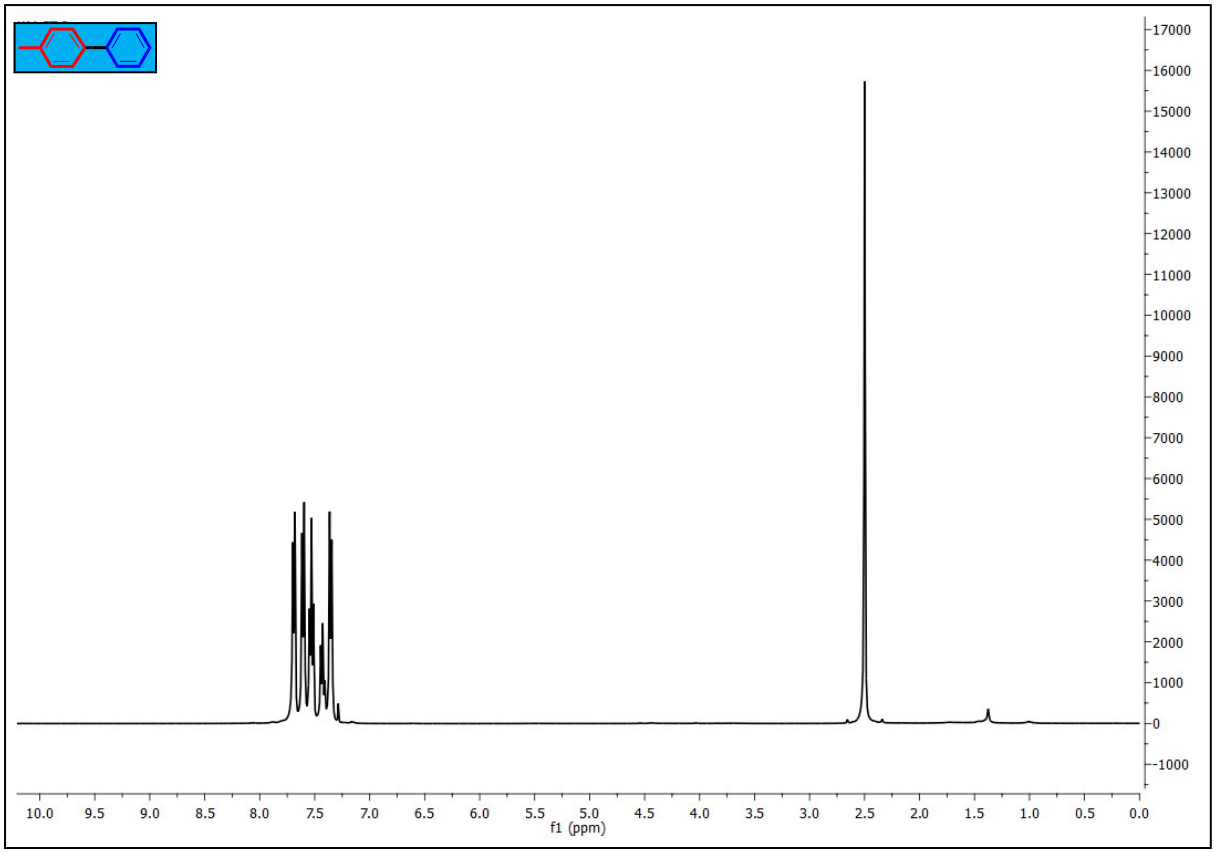

S28 ^{1}H NMR of Entry 1(Table 6)

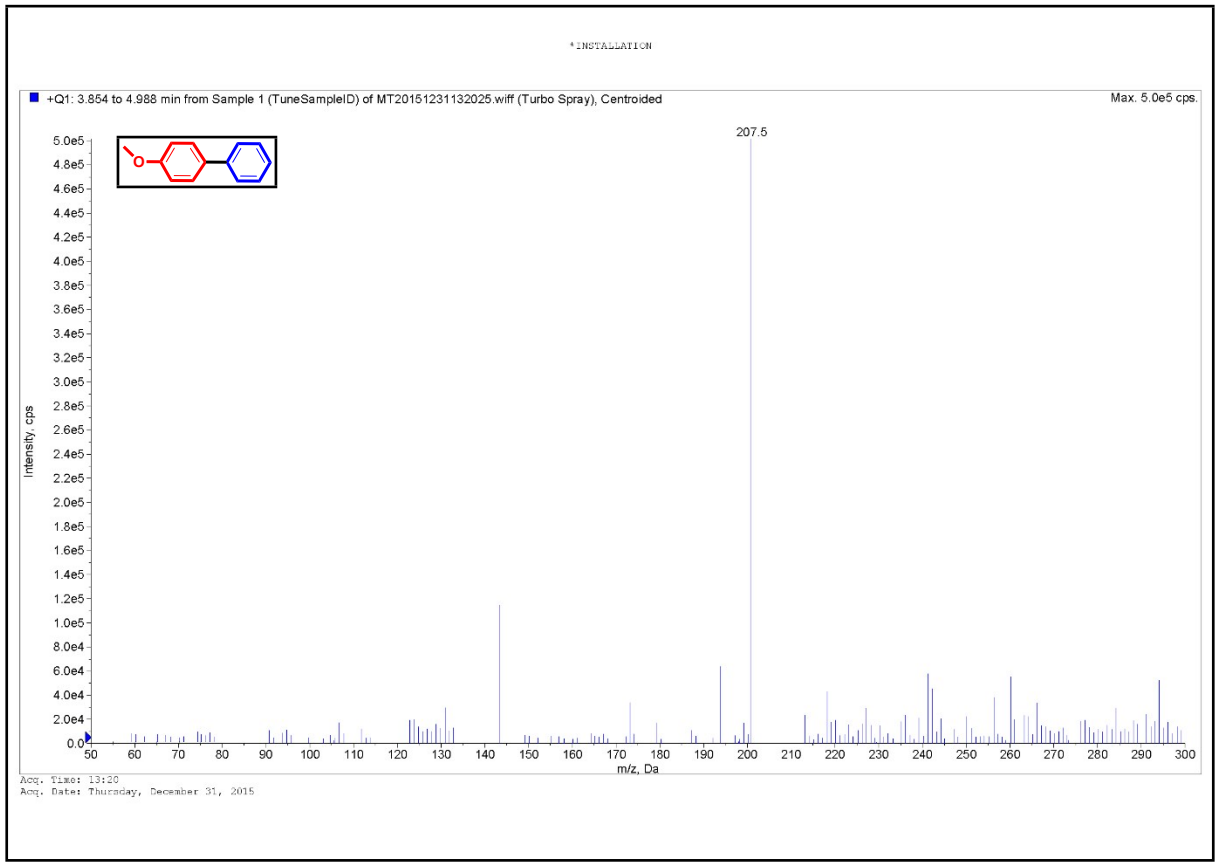

S29 Mass of Entry 2(Table 6)

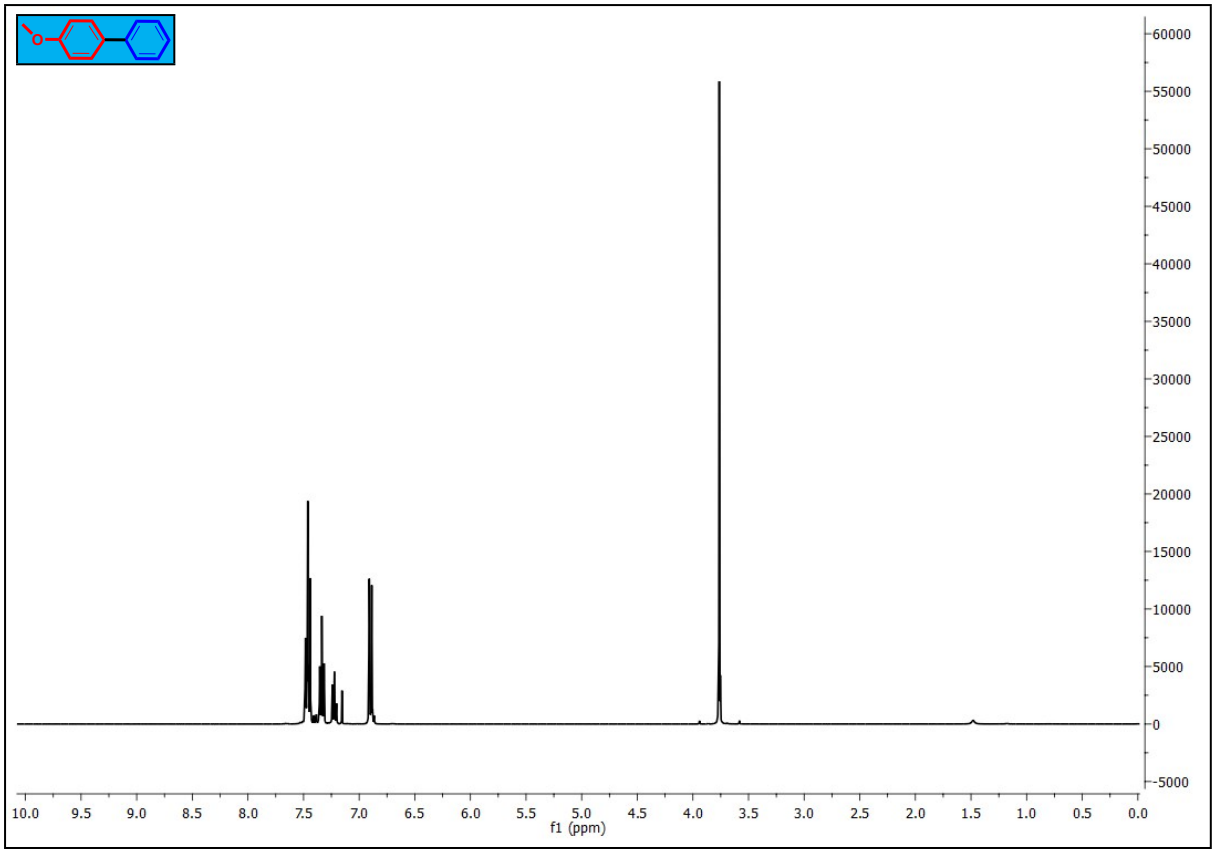

S30 ^{1}H NMR of Entry 2(Table 6)

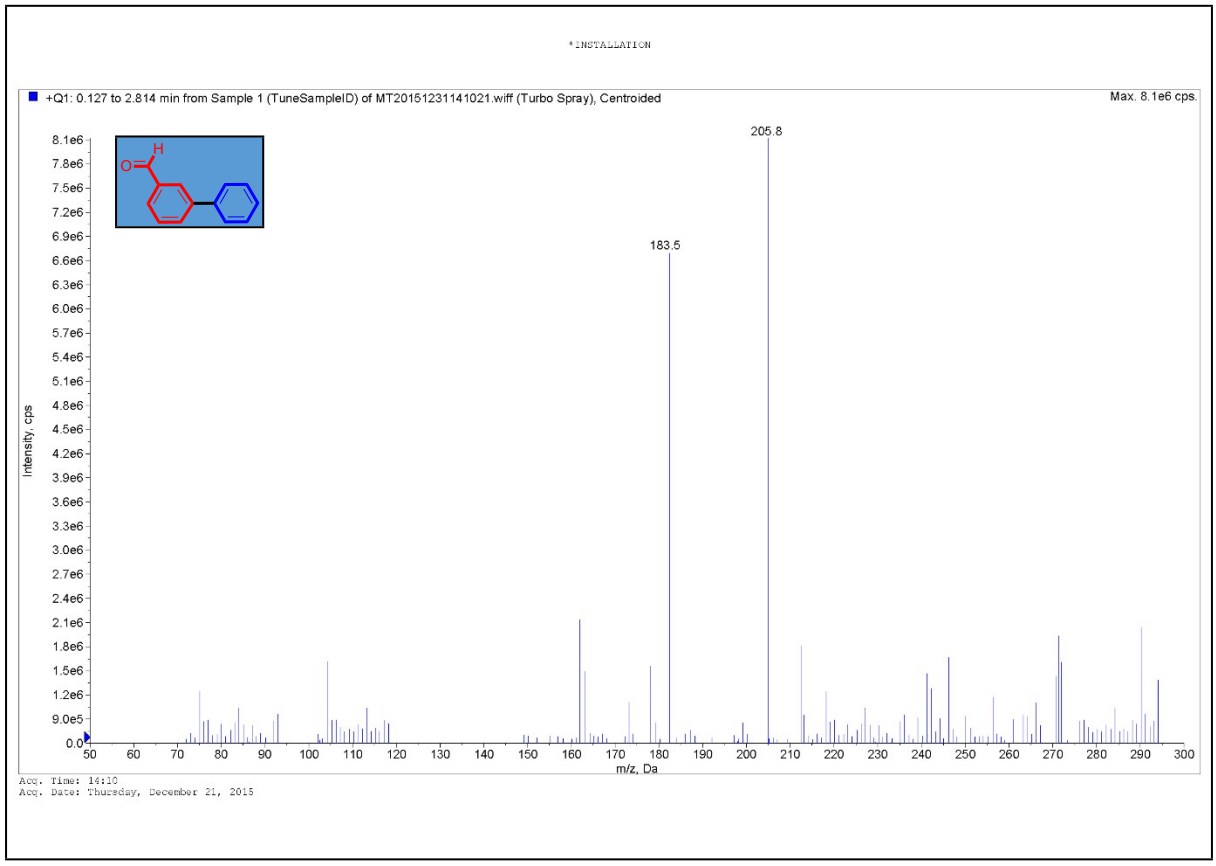

S31 Mass of Entry 3(Table 6)

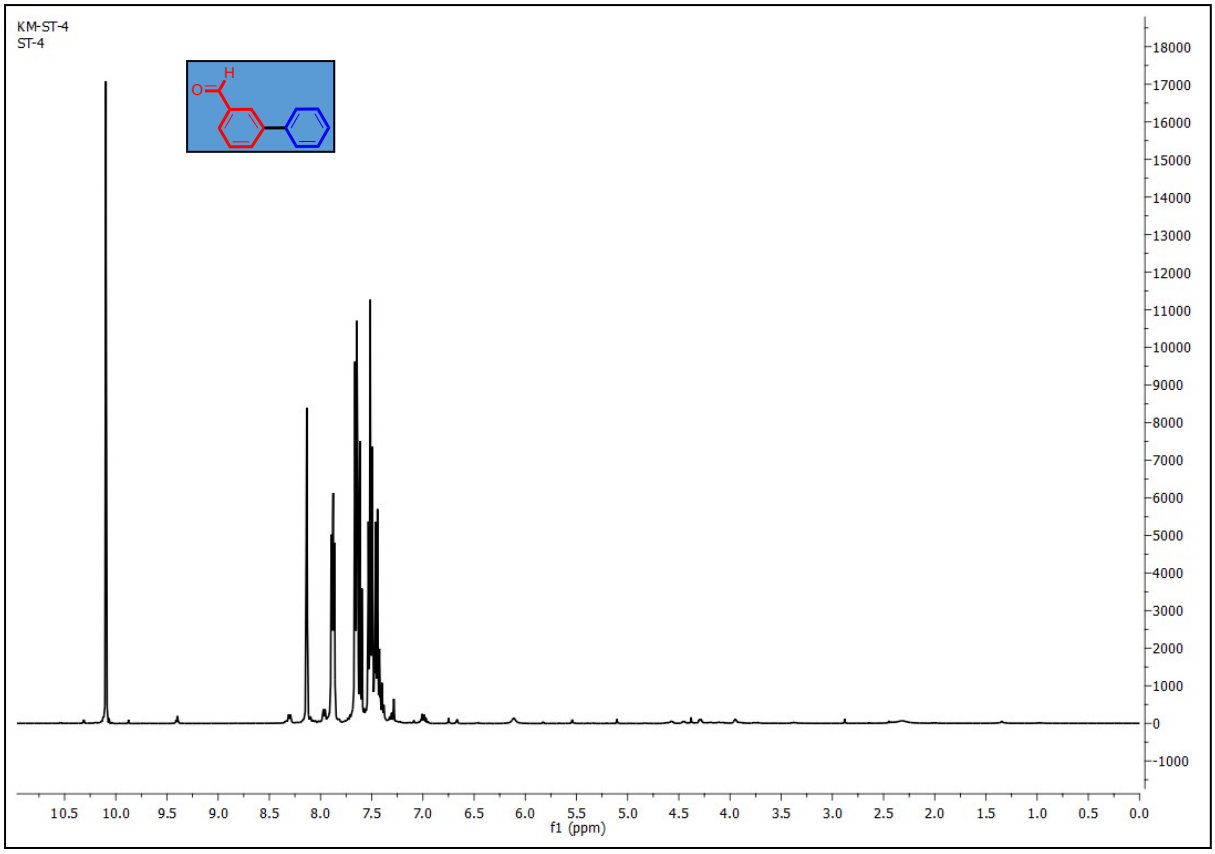

S32 ^{1}H NMR of Entry 3(Table 6)

S33 Optimization details

Sr. No	Name	Method	Basis set	Optimization Energy			
				Gas Phase		Solvent Phase*	
				Opti. Step	Energy	Opti. Step	Energy
1	TPA	HF	6-31g(d,p)	24	-3725.925665	15	-3725.942204 [a]
		B3LYP	6-31g(d,p)	28	-3742.13554	8	-3742.135543 [a]
		HF	6-311g(d,p)	17	-3726.397402	40	-3726.414499 [a]
		B3LYP	6-311g(d,p)	17	-3742.699881	17	-3742.713271 [a]
2	TPTAE	HF	6-31g(d,p)	4	-4944.709334	76	-4944.743183 [a]
		B3LYP	6-31g(d,p)	150	-4968.065264	49	-4968.092963 [a]
		HF	6-311g(d,p)	21	-4945.446387	40	-4945.480496 [a]
		B3LYP	6-311g(d,p)	56	-4968.924728	32	-4968.955122 [a]
3	TPTAH	HF	6-31g(d,p)	95	-4773.097305	48	-4773.146277 [b]
		B3LYP	6-31g(d,p)	105	-4795.393777	52	-4795.434472 [b]
		HF	6-311g(d,p)	42	-4773.805815	56	-4773.855202 [b]
		B3LYP	6-311g(d,p)	43	-4796.223313	116	-4796.265928 [b]

*a=Chloroform; b=Water

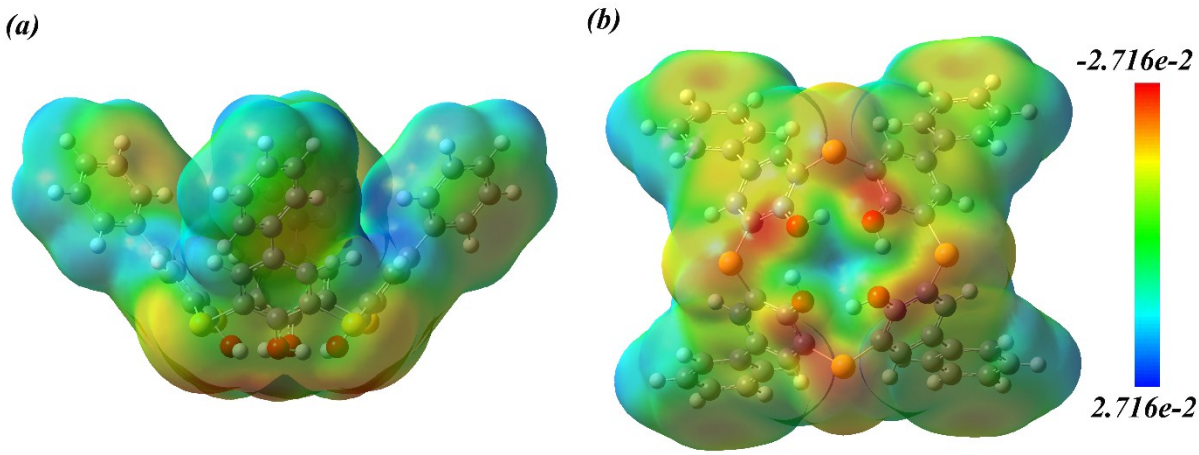

S34 Mapped Molecular Electrostatic potential from the electron density (total SCF density; isoval=0.0004) (a) Front view, (b) Bottom view of various atoms of TPA at B3LYP/6-311G (d,p) level

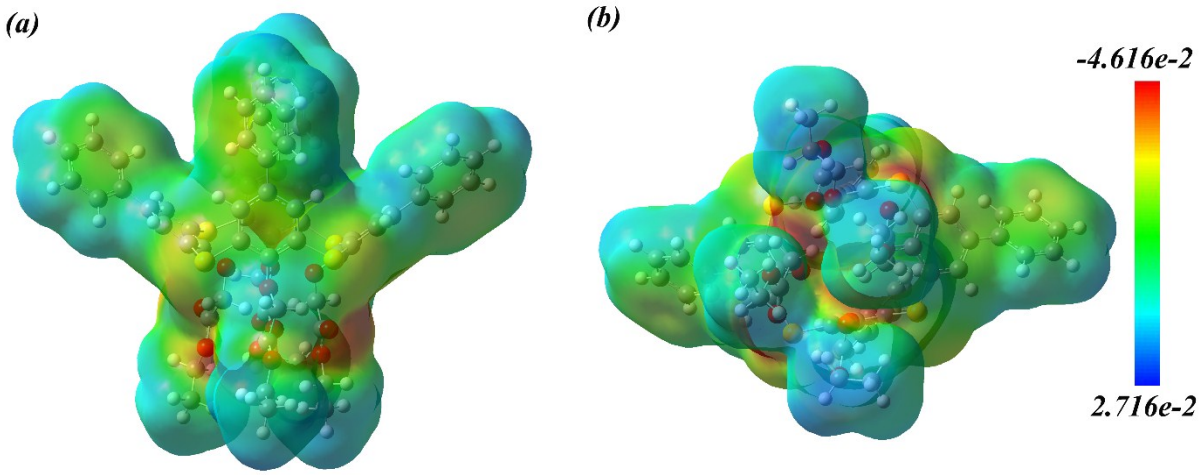

S35 Mapped Molecular Electrostatic potential from the electron density (total SCF density; isoval=0.0004) (a) Front view, (b) Bottom view of various atoms of TPTAE at B3LYP/6-311G (d,p) level

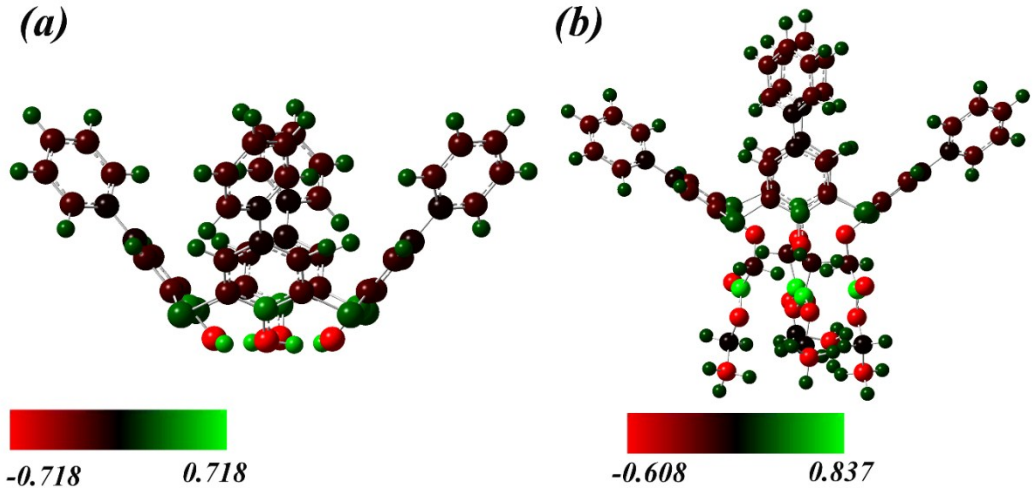

S36 Natural Bond Orbital (NBO) charges of various atoms of (a) TPA, (b) TPTAE at B3LYP/6-311G (d,p) level

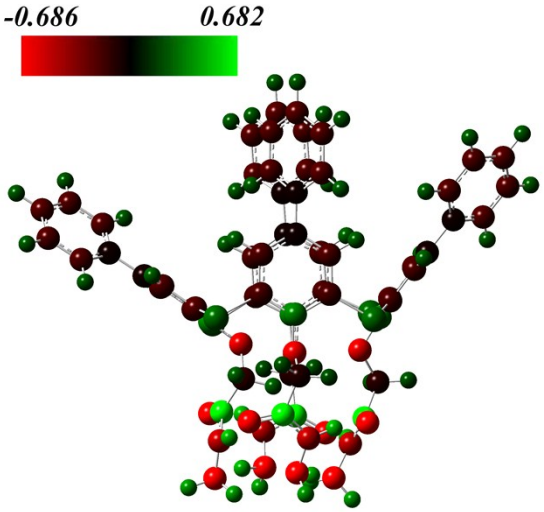

S37 Natural Bond Orbital (NBO) charges of various atoms of TPTAH at B3LYP/6-311G (d,p) level

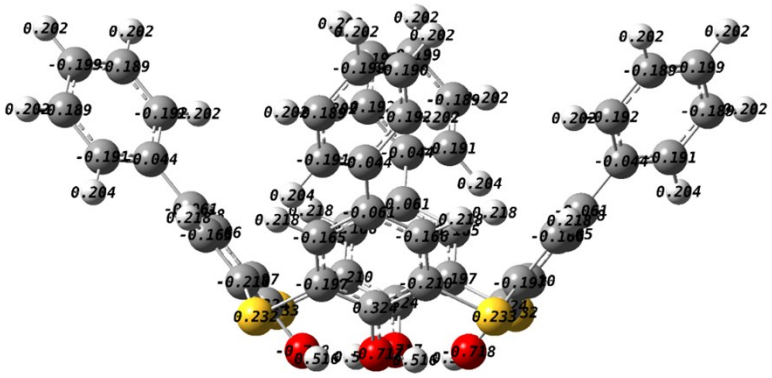

S38 Natural Bond Orbital (NBO) charges of various atoms of TPA at B3LYP/6-311G (d,p)

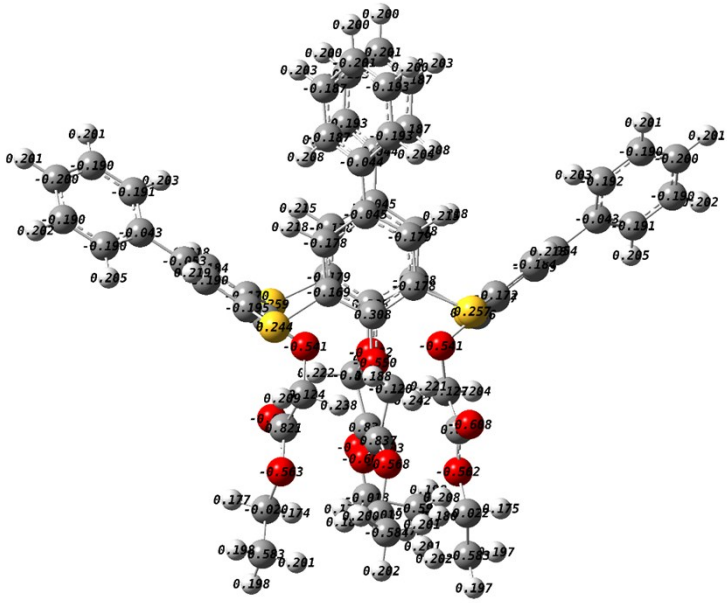

S39 Natural Bond Orbital (NBO) charges of various atoms of TPTAE at B3LYP/6-311G (d,p)

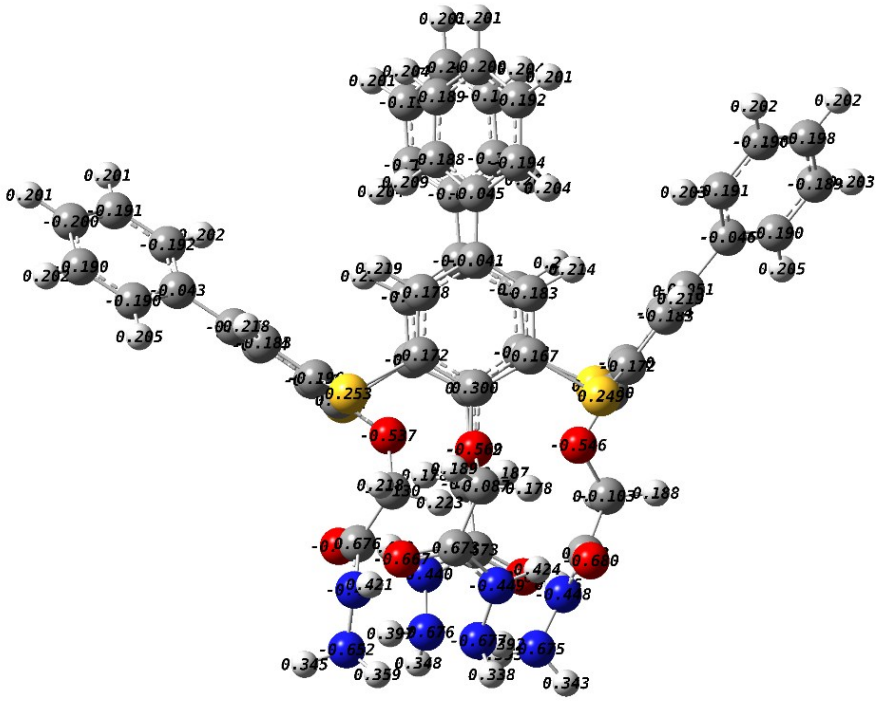

S40 Natural Bond Orbital (NBO) charges of various atoms of TPTAH at B3LYP/6-311G (d,p)

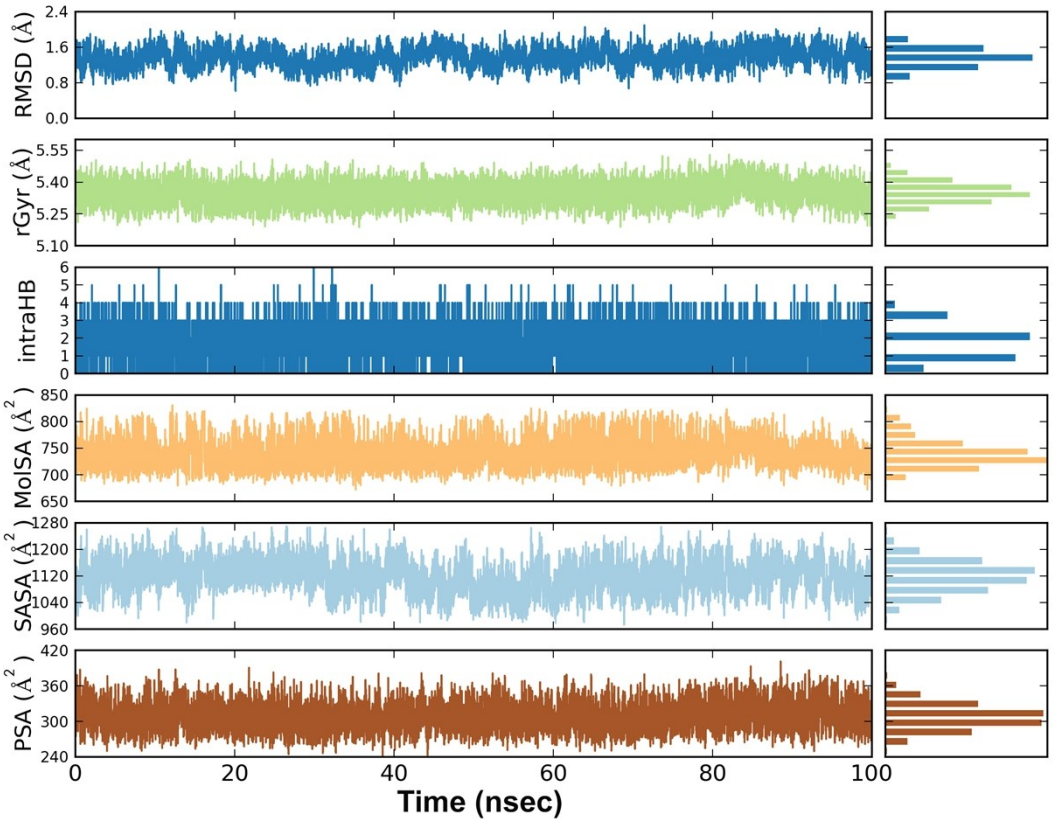

S41 Simulation interaction analysis through RMSD (Root mean square deviation of a ligand); rGyr (Radius of Gyration); intra Hydrogen bond; MolSA (Molecular Surface Area); SASA (Solvent Accessible Surface Area) and PSA (Polar Surface Area)

S42 Optimization details for TPTAH_PdNps

Sr. No	Name	Method	Basis set	Optimization Energy at Solvent Phase*		
				Opti. Step	Predicted Energy change	Energy (Hatree)
1	TPTAH	HF	6-31g(d,p)	48	-1.84E-08	-4773.146277
2	Pd_cluster	HF	SDD	13	-1.51E-07	-1778.681973
3	TPTAH_PdNps	HF	Gen†	259	-2.11E-08	-6551.925885

*Water; † 6-31g(d,p)/SDD

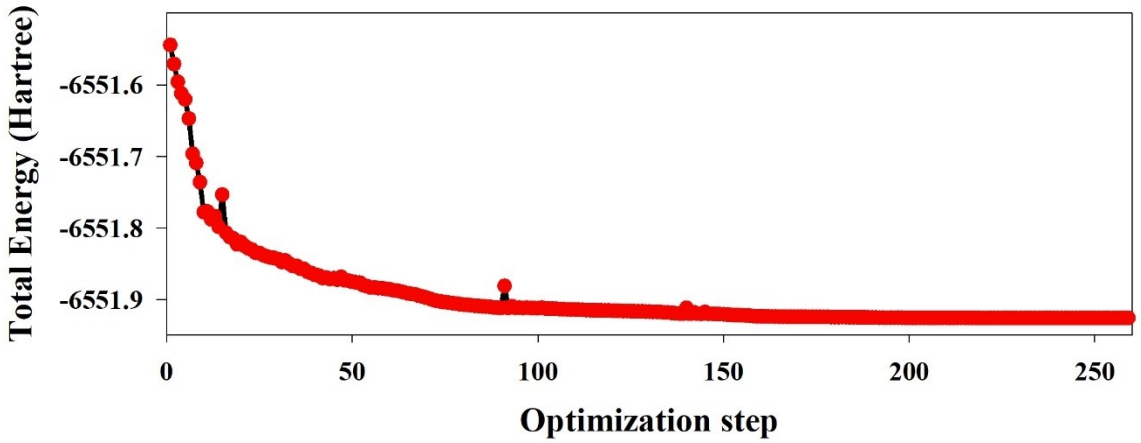

S43 Geometry optimization graph of Total energy of TPTAH_PdNps@ HF/Gen

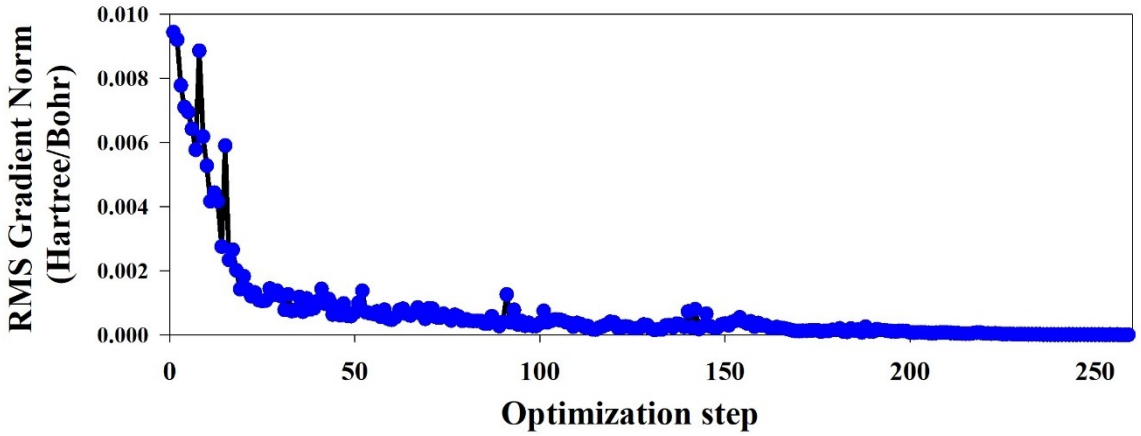

S44 Geometry optimization graph of RMS Gradient Norm of TPTAH_PdNps@ HF/Gen

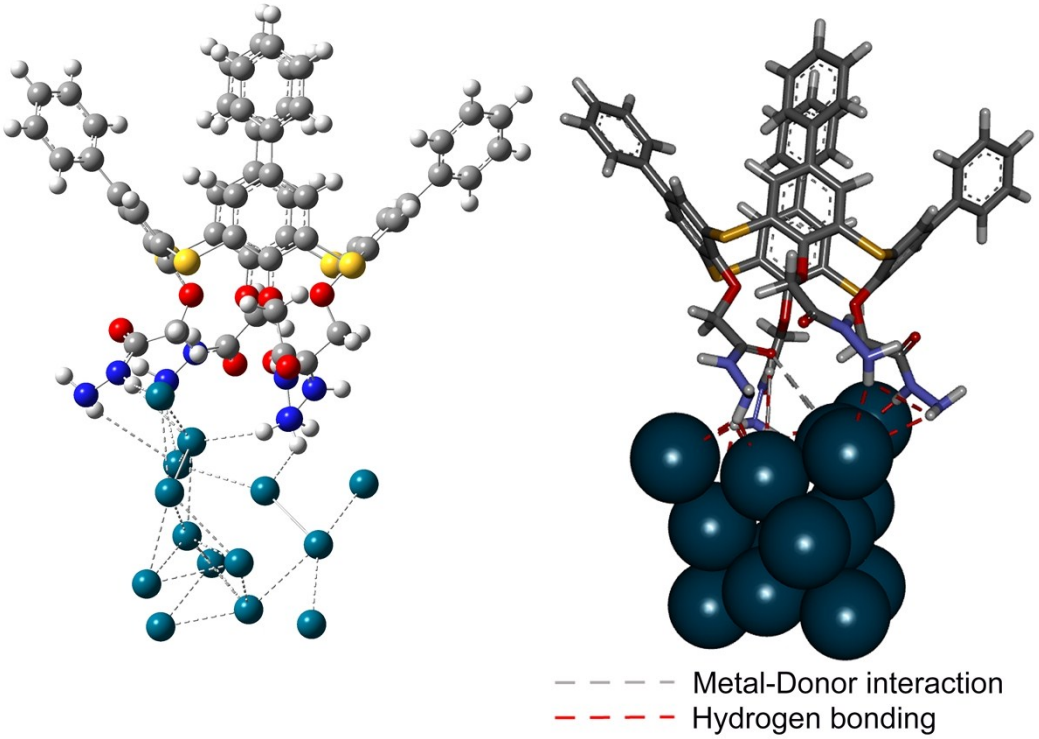

S45 TPTAH_PdNps interactions after DFT optimization at HF/6-31G (d,p) level of approximation

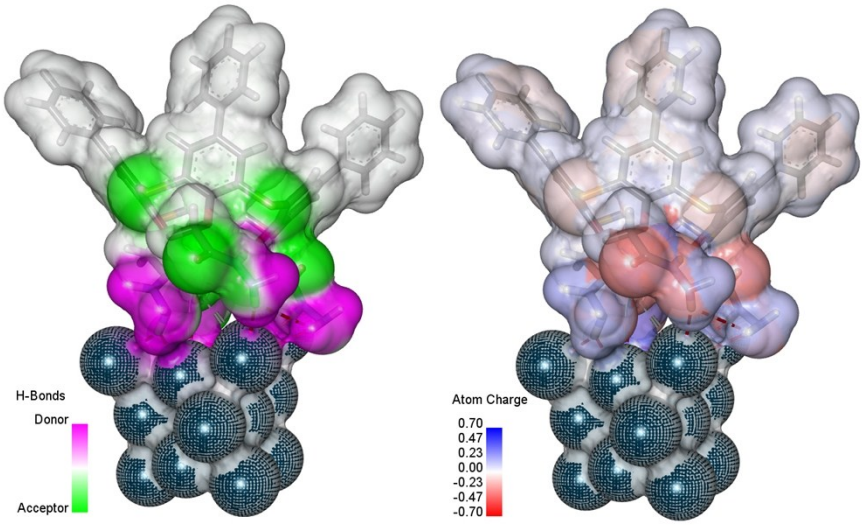

S46 TPTAH_PdNps donor-acceptor interactions and atom charges after DFT optimization at HF/6-31G (d,p) level of approximation

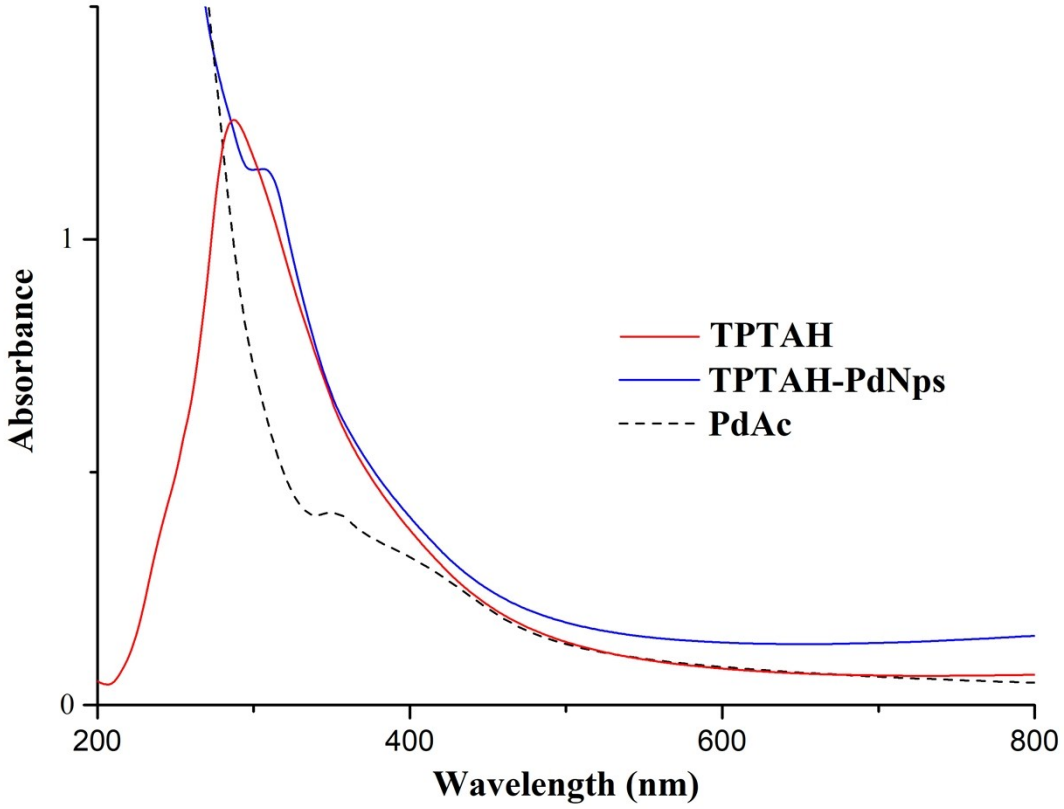

S47 UV-Vis Spectra of TPTAH, TPTAH-PdNPs, and PdAc

References:

1. M. Frisch, G. Trucks, H. Schlegel, G. Scuseria, M. Robb, J. Cheeseman, G. Scalmani, V. Barone, B. Mennucci and G. Petersson, *Gaussian Inc., Wallingford, CT*, 2009.
2. K. J. Bowers, D. E. Chow, H. Xu, R. O. Dror, M. P. Eastwood, B. A. Gregersen, J. L. Klepeis, I. Kolossvary, M. A. Moraes, F. D. Sacerdoti, J. K. Salmon, Y. Shan and D. E. Shaw, 2006.
3. W. L. Jorgensen and J. Tirado-Rives, *Journal of the American Chemical Society*, 1988, **110**, 1657-1666.
4. E. Harder, W. Damm, J. Maple, C. Wu, M. Reboul, J. Y. Xiang, L. Wang, D. Lupyan, M. K. Dahlgren, J. L. Knight, J. W. Kaus, D. S. Cerutti, G. Krilov, W. L. Jorgensen, R. Abel and R. A. Friesner, *Journal of Chemical Theory and Computation*, 2016, **12**, 281-296.
5. U. Essmann, L. Perera, M. L. Berkowitz, T. Darden, H. Lee and L. G. Pedersen, *The Journal of Chemical Physics*, 1995, **103**, 8577-8593.
6. L. Ray, S. Barman, M. M. Shaikh and P. Ghosh, *Chemistry–A European Journal*, 2008, **14**, 6646-6655.
7. A. J. Canty and A. Ariafard, *Journal of Organometallic Chemistry*, 2018, **872**, 110-113.
8. D. S. Visualizer, *Accelrys Inc, San Diego, CA, USA*, 2012.